A&A 377, 538–556 (2001)
DOI: 10.1051/0004-6361:20011093


Astronomy & Astrophysics

# X-ray emission from young stars in Taurus-Auriga-Perseus: Luminosity functions and the rotation – activity – age – relation⋆

B. Stelzer and R. Neuhäuser

Max-Planck-Institut für extraterrestrische Physik, Postfach 1312, 85741 Garching, Germany

Received 4 September 2000 / Accepted 26 July 2001

**Abstract.** We report on a systematic search for X-ray emission from pre-main sequence and young main sequence stars in the Taurus-Auriga-Perseus region. Our stellar sample consists of all T Tauri stars from the Taurus-Auriga region, and all late-type stars from the Pleiades and Hyades clusters which have been observed by the *ROSAT* PSPC in pointed observations. We present the X-ray parameters for all observed stars in tables. Next to the basic results of the data analysis (such as count rates, exposure time, and off-axis angle) we give X-ray luminosities and hardness ratios for all detected stars. Upper limits are given for non-detections. Detection rates for different spectral types are compiled. We use these results to study the connection between coronal X-ray activity and stellar parameters for different subgroups of our sample. In particular we compile X-ray luminosity functions (XLF), and discuss the relations between X-ray emission and spectral type, age, and rotation, which have been disputed extensively in the past. Here, we study these questions with the largest sample so far. The XLF for classical and weak-line T Tauri stars are different, with weak-lines being the stronger X-ray emitters. Proceeding towards the main-sequence (Pleiades, Hyades) the X-ray luminosity declines for all spectral types examined (G, K, and M stars). Within an age group $L_{\rm x}$ decreases towards later spectral types, while $L_{\rm x}/L_{\rm bol}$ remains constant or even increases, reflecting the opposed influence of stellar radius, i.e. emitting area, and convection zone depth. For a given spectral type the fastest rotators show the highest X-ray luminosity. Rotation rate and X-ray emission are clearly correlated for all groups of stars with power law indices for $\log(L_{\rm x}/L_{\rm bol})$ versus $\log P_{\rm rot}$ of $\sim -0.7$ to $-1.5$. The study of XLF for binary stars shows that the known unresolved secondaries likely contribute a significant amount to the X-ray emission.

**Key words.** X-rays: stars – stars: late-type, pre-main sequence, coronae, activity

## 1. Introduction

Late-type stars are known to sustain a dynamo which is powered by the combination of convective motions and rotation. The resulting magnetic field is thought to be responsible for various observational phenomena commonly referred to as "activity". Stellar activity indicators are pervasive in all layers of the atmospheres of late-type stars. The best-studied magnetic field tracers include chromospheric H$\alpha$ and Ca II emission lines and coronal X-rays.

Strong and variable X-ray emission is observed from the early pre-main sequence (PMS) T Tauri stage to main sequence flare stars. Comparative studies of the emission levels of young stars at different ages may shed light on the origin and evolution of magnetic activity, which may be linked to angular momentum evolution.

T Tauri Stars (TTS) are divided into two subclasses according to the strength of their H$\alpha$ emission. Classical TTS (cTTS) are characterized by strong H$\alpha$ emission, while in weak-line TTS (wTTS) the equivalent width of H$\alpha$ is smaller than 10 Å. In contrast to cTTS, wTTS do not show obvious signs of accretion and optically thick disks, and therefore are thought to represent a later evolutionary stage at which the circumstellar disk has become optically thin or dispersed. Nevertheless, some wTTS occupy the same region in the Hertzsprung-Russell diagram as the cTTS (see e.g. Walter et al. 1988; Alcalá et al. 1997), i.e. there seems to be no preferred disk lifetime between several $10^5$ and $10^7$ yrs.

During the PMS contraction stars gain angular momentum and should spin up. However, cTTS show much slower rotation rates than wTTS (Bouvier et al. 1993) despite their high accretion rates. This can be explained by magnetic coupling between the star and the disk in cTTS which allows to regulate angular momentum transport without spinning up the star (Koenigl 1991; Edwards et al. 1993; Bouvier et al. 1997a).

*Send offprint requests to*: B. Stelzer,
e-mail: stelzer@xray.mpe.mpg.de

⋆ Tables 2 to 7 are only available in electronic form at http://www.edpsciences.org

The strength of activity is thought to decline with increasing stellar age. Skumanich et al. (1972) have proposed a $1/\sqrt{t}$-law for the decay of stellar activity in young stellar clusters based on Ca II line observations. The power-law relation was confirmed by Feigelson & Kriss (1989) for a sample including PMS objects in Chamaeleon. However, the study of Walter et al. (1988) seemed to indicate that during the PMS phase the X-ray emission remains nearly constant, while for ages $\geq 10^8$ yrs it decays exponentially. Walter & Barry (1991) have argued that a power-law decay may be an artefact that occurs when the X-ray luminosity is used as activity indicator in a sample composed of stars with different stellar radii. Using the surface flux Walter & Barry (1991) have shown that the decay of various activity diagnostics probing the lower chromosphere, transition region, and corona can be described by an exponential.

An evolutionary decay of the X-ray emission is favored also by studies of the *Einstein* Observatory (*EO*) which have shown that the X-ray luminosity functions (XLF) of stellar clusters with different ages are displaced from each other (see e.g. Feigelson & Kriss 1989; Damiani et al. 1995). However, rather than being a pure age effect, the decreasing activity (i.e. the decay of the dynamo efficiency) might be explained by the slowing down of the rotation with increasing age on the main sequence (MS). A connection between the dynamo efficiency and the rotation rate is also supported by correlations between the X-ray activity and the rotational velocity (see Pallavicini et al. 1981; Bouvier 1990; Neuhäuser et al. 1995 = N95) found to hold for all kinds of active stars, featuring such different objects like dMe stars, RS CVn binaries, and TTS. For the fastest rotators among the Pleiads (Stauffer et al. 1994) and among the wTTS (Damiani & Micela 1995) the relation flattens out suggesting "saturation" of the X-ray emission at very high rotation speeds. Stauffer et al. (1994) have proposed that the large spread observed in the X-ray luminosities of slower rotators are caused when more and more stars leave the saturation level thus increasing the dispersion. A later study by Micela et al. (1996) showed no significant correlation between $L_{\rm x}$ and $v \sin i$ for Pleiades stars, indicating that rotation can not be the only parameter governing the X-ray emission level of young stars. To date, no solution has been found to the question whether age or rotation determines the level of stellar activity.

If rotation does determine the activity, then cTTS should show lower X-ray luminosities than wTTS. XLF provide a statistical tool to compare the X-ray properties of different stellar samples. But so far, studies of the XLF of cTTS and wTTS have not led to a conclusive result concerning the evolution of X-ray activity during the PMS. N95 have shown that X-ray emission increases with age from cTTS to wTTS, but decreases after the wTTS phase. While N95 found that wTTS in Taurus-Auriga emit significantly more X-rays as compared to cTTS from the same region, Feigelson et al. (1993) found little evidence for systematic differences in the XLF of wTTS and cTTS in Chamaeleon, and argued that the differences in the X-ray luminosity between wTTS and cTTS in Taurus-Auriga might be attributed to as yet undicovered wTTS at the low-luminosity end of the distribution.

In this paper we examine the connection between X-ray activity, age, and rotation comparing different samples of young stars. The Taurus-Auriga-Perseus region is well suited for a study of the evolution of stellar activity because it hosts a large number of young stars at different ages: the molecular clouds of Taurus-Auriga are sites of ongoing star formation and have produced many TTS with ages between several $10^5$ to $10^7$ yrs. Besides this star forming region, two young star clusters are located in the area, the Pleiades and the Hyades, at ages of $10^8$ yrs and $6 \times 10^8$ yrs respectively.

Our sample is larger and the sensitivity improved compared to all previous studies of this issue. The paper presented here is connected to an earlier analysis of archived *ROSAT* observations (Stelzer et al. 2000). Here we present a list of X-ray parameters for all known TTS in Taurus-Auriga, the Pleiades, and the Hyades as observed by *ROSAT* during pointed PSPC observations. Both detected and undetected sources are considered, i.e. for non-detections upper limits are given. In Sect. 2 we describe the data base and data reduction and give the results from source detection. In Sect. 3 the Hertzsprung-Russell diagrams (H-R diagrams) for cTTS and wTTS in Taurus-Auriga are presented. Our special interest (Sect. 4) is to compare the XLF of the different stellar groups with respect to the following issues: (i) Are the luminosity functions of cTTS and wTTS different, (ii) how does the X-ray luminosity evolve with stellar age, (iii) how does it depend on the spectral types of the stars and their binary character. Furthermore, we will explore the relation between X-ray emission and rotation rate for the largest sample studied so far (Sect. 5). In Sect. 6 we discuss and summarize our results.

## 2. Observations

### 2.1. Data base

The sky region examined is confined to the Taurus-Auriga-Perseus area. A detailed description of this region is given in Stelzer et al. (2000) (hereafter SNH00) where we have also presented a sky map showing the *ROSAT* PSPC observations subject to this and the previous study. The stellar sample investigated in this paper is identical to the one described in SNH00. However, we omit stars from the Perseus clouds IC 348 (Preibisch et al. 1996) and NGC 1333 (Preibisch 1997), since due to their larger distance the PSPC images are dominated by source confusion. We analyse the X-ray emission of young, late-type stars, represented by TTS and members from the Pleiades and Hyades clusters. The selection of the Pleiades and Hyades as examples of young clusters was motivated by their spatial vicinity to the Taurus-Auriga molecular clouds when projected to the sky. For this reason many

Pleiads and Hyads lie in the same *ROSAT* PSPC fields. Most of the X-ray detected Pleiads and Hyads are zero-age main-sequence (ZAMS) stars. There are also some (higher-mass) post-MS stars which are not studied here, and many PMS brown dwarfs. The sample examined extends down to the latest M-type objects and includes brown dwarf candidates. Most of these are below the detection limit. However, we have detected an M9-type object in Taurus-Auriga, the latest type PMS dwarf seen to emit X-rays so far (see Sect. 2.5). The coolest object detected in the Pleiades has spectral type M5. In the Hyades we detect objects down to M9 (spectral types determined from measurements of $B-V$). With their different ages the three groups of stars (TTS, Pleiads, and Hyads) allow to examine the evolution of the X-ray luminosity.

We have selected all pointed PSPC observations from the *ROSAT* Public Data Archive available in October 1998 which contain any TTS in the Taurus-Auriga region, any Pleiad, or any Hyad in the field of view. The TTS in that area of the sky are part of the Taurus-Auriga molecular clouds located at 140 pc (Elias 1978; Wichmann et al. 1998a). For the distance to the Pleiades cluster we have adopted 116 pc, the value given by Mermilliod et al. (1997). Those Hyades stars for which no individual Hipparcos parallaxes are available are assumed to be at a distance of 46 pc (Perryman et al. 1998).

A detailed description of the membership lists for TTS, Pleiads, and Hyads is given in SNH00. SNH00 also have presented a complete list of the pointed *ROSAT* PSPC observations analysed here. In the earlier paper we were dealing with the same observations but have concentrated on large X-ray flares observed on detected stars. Now we discuss the X-ray characteristics of the whole sample, including non-flaring stars and non-detections. Therefore, we also analyse the short exposures and observations with unstable background marked with an asterisk in Table 1 of SNH00, and not considered in that earlier investigation.

### 2.2. Source detection

Source detection is performed based on a maximum likelihood method which combines local and map source detection algorithm (see Cruddace et al. 1988). Sources with a $ML \geq 7.4$ (corresponding to $\sim$3.5 Gaussian $\sigma$ and shown to be the best choice by N95) are considered to be a detection. The probability for existence of a source of given $ML$ is given by $P = 1 - \exp(-ML)$. For $ML = 7.4$ the probability is 0.9994, and among the $\sim$800 detected young stars we would expect to find less than one spurious source.

Observations whose center positions are less than $15''$ apart have been merged to increase the sensitivity for faint detections. The photon extraction radius of the X-ray sources is not well defined if the off-axis positions in individual observations that are merged differ strongly from each other. Therefore, we have analysed observations with less overlap, i.e. more than $15''$ separation, separately. The center of the merged image is the center from all individual observations that are added up. The off-axis positions of X-ray sources in merged pointings are computed with respect to this averaged pointing position.

**Table 1.** Maximum offset allowed between optical and X-ray position $\Delta_{\rm ox,max}$ for different off-axis angles $\Omega$. $\Delta_{\rm ox,max}$ is the best-fit value of a linear distribution of offsets found from normalized cumulative numbers of identifications (see text).

| Off-axis angle [arcmin] | | | | | $\Delta_{\rm ox,max}$ [arcsec] |
|---|---|---|---|---|---|
| | | $\Omega$ | $\leq$ | 27.5 | 40.0 |
| 27.5 | $<$ | $\Omega$ | $\leq$ | 30 | 42.4 |
| 30 | $<$ | $\Omega$ | $\leq$ | 32.5 | 49.5 |
| 32.5 | $<$ | $\Omega$ | $\leq$ | 35 | 56.7 |
| 35 | $<$ | $\Omega$ | $\leq$ | 37.5 | 63.8 |
| 37.5 | $<$ | $\Omega$ | $\leq$ | 40 | 70.9 |
| 40 | $<$ | $\Omega$ | $\leq$ | 42.5 | 78.1 |
| 42.5 | $<$ | $\Omega$ | $\leq$ | 45 | 85.2 |
| 45 | $<$ | $\Omega$ | $\leq$ | 47.5 | 92.3 |
| 47.5 | $<$ | $\Omega$ | $\leq$ | 50 | 99.5 |

As the positional accuracy of the *ROSAT* PSPC declines towards the edge of the detector, the identification radius between optical and X-ray position depends on the off-axis angle of the source. We have computed the normalized cumulative number of identifications as a function of the offset between optical and X-ray position, $\Delta_{\rm ox}$, for different ranges of off-axis angles. Following N95, for each of these distributions we have determined the turnover point, $\Delta_{\rm ox,max}$, which corresponds to the value of $\Delta_{\rm ox}$ where wrong identifications begin to contribute significantly to the detected sources. We have then performed a linear fit to the mean off-axis angle as a function of this critical offset $\Delta_{\rm ox,max}$. The fit values of $\Delta_{\rm ox,max}$ for all examined off-axis ranges are listed in Table 1. These values are used as identification radii for the cross-correlation of membership lists and X-ray observations. For off-axis angles below $27.5'$ a maximum offset between optical and X-ray position of $40''$ is appropriate. Note, that this value agrees with the value found by N95 for the *ROSAT* All-Sky Survey (RASS). Sources which are located further than $50'$ from the detector center are ignored in the analysis presented here, because at large off-axis angles the point spread function deviates from a Gaussian and can not be adequately modeled by the available software.

We have computed the count rates of detected and undetected sources by integrating all events within a circular region around the source position, i.e. the X-ray position for detections and the optical position for non-detections. We use the 99% quantile of the point spread function at 1 keV as photon extraction radius, except for those few cases where the broad band X-ray image shows that the source obviously exceeds this radius probably due to the energy being different from 1 keV. For these special cases we determine the optimum radius individually by visual inspection of the X-ray image.

The measured counts are background subtracted and divided by the exposure time obtained from the exposure

map to determine the count rates. For the background subtraction we have used the information from the background maps. This method is useful in crowded fields where a background annulus around the source may easily be contaminated by adjacent sources.

In the crowded Pleiades region occasionally two or more X-ray sources show significant overlap. In order to separate the contributions from each star we were forced to decrease the photon extraction radius of these sources. This leads to an underestimation of the true count rate, but should not effect our results due to the low number of confused stars (15 versus >200 detections among the Pleiades).

### 2.3. Results of source detection

The result of source detection and identification is summarized in six tables: Tables 2, 3, and 4 contain the X-ray parameters of all detected TTS, Pleiads, and Hyads, and in Tables 5, 6, and 7 the X-ray characteristics of undetected TTS, Pleiads, and Hyads are listed.

In Tables 2–7 the first column contains a number for the observation referring to the numbering in Table 1 in SNH00. (See SNH00 for the *ROSAT* observation request numbers.) For merged observations we give the numbers of all pointings that have been added up. Column 2 is the designation of the stars. Column 3 contains two flags, one that gives the type of TTS ("W" – wTTS, "C" – cTTS) and another one for the multiplicity of the stellar system ("S" – single, "B" – binary, "T" – triple, and "Q" – quadruple). The distinction between cTTS and wTTS is based mainly on the standard H$\alpha$ equivalent width boundary of 10 Å together with the spectral type of the star (i.e. the H$\alpha$ flux), which is similar to the suggestion by Martín (1997) to use different $W_{\mathrm{H}\alpha}$ boundaries for different spectral types (GKM). Furthermore, we make use of indications for circumstellar material as revealed from IR and mm observations. SU Aur, e.g., is of spectral type G2 and $W_{\mathrm{H}\alpha}$ is between 3.5 and 5 Å, but it also has a massive disk and, therefore, clearly is a cTTS. The H$\alpha$ equivalent widths are taken from N95, Kenyon & Hartmann (1995), and Wichmann et al. (1996). The spectral types are shown in Col. 4. The spectral types of Pleiades and Hyades stars were derived from the $B-V$ measurements given in the Open Cluster Data Base compiled by C. Prosser and colleagues (and available at `ftp://cfa-ftp.harvard.edu/pub/stauffer/clusters`) using the conversion of Schmidt-Kaler (1982). For TTS in Taurus-Auriga we have adopted the spectral types compiled by N95 and König et al. (2001).

For all detected stars (Tables 2–4) we list the X-ray position (Cols. 5 and 6), the offset $\Delta$ between optical and X-ray position (Col. 7), the off-axis angle (Col. 8), and the maximum likelihood (Col. 9) of existence. We give the X-ray hardness ratios $HR1$ and $HR2$ in Cols. 10 and 11. The PSPC hardness ratio $HR1$ is defined as follows:

$$HR1 = \frac{H-S}{H+S} \tag{1}$$

where $H$ is the hard band count rate between 0.5–2.0 keV, and $S$ is the count rate in the soft band (between 0.1–0.4 keV). $HR2$ is given by:

$$HR2 = \frac{H2-H1}{H2+H1} \tag{2}$$

where $H2$ and $H1$ are the count rates in the upper and lower part of the hard band between 0.5–0.9 keV ($H1$) and 0.9–2.0 keV ($H2$), respectively. In cases where no counts are observed in any one energy band, and therefore $HR1$ or $HR2$ are either +1.0 (no soft counts) or −1.0 (no hard counts) we have computed upper limits to the hardness from the counts in the background. Column 12 gives the exposure time and Col. 13 the X-ray luminosity.

In order to determine the count-to-energy-conversion-factor $CECF$ for the compilation of luminosities we have used the hardness criterion given by Fleming et al. (1995): $CECF = (8.31+5.30\cdot HR1)\times 10^{-12}\,\mathrm{erg\,cm^{-2}\,cts^{-1}}$. Since the soft band in $HR1$ is sensitive to $A_V$, this way we implicitly take account of the extinction. It should be noted that $HR1$ "saturates" for extinctions $A_V > \sim 0.5$. High extinctions are however rare in the Taurus region, and do not play a role for the Pleiades and Hyades. But to ensure that no systematic errors are introduced by this method of count-to-energy conversion we have compared the resulting distribution of X-ray luminosities with those directly derived from the available $A_V$ measurements (see Sect. 4.1).

The values of the luminosity given in Tables 2–4 have been derived dividing the count rate by the multiplicity of the stellar system. This means we assume that each of the components in the system contributes the same level of X-ray emission (see König et al. 2001 and Sect. 4.3). The mean value of the $CECF$ is $1.00 \pm 0.25 \times 10^{-11}$ erg cm$^{-2}$ cts$^{-1}$. This value was used to obtain the luminosity in cases where $HR1$ is a upper/lower limit, and therefore Fleming's relation cannot be applied. Uncertainties in $\log L_{\mathrm{x}}$ are derived from the statistical errors without taking account of systematic uncertainties in the distance estimate.

X-ray parameters for non-detections are summarized in Tables 5–7. The meaning of Cols. 1 to 4 in Tables 5–7 is the same as in Tables 2–4. In Cols. 5 and 6 we list the optical position. The off-axis angle of the undetected stars is given in Col. 7. Column 8 contains the upper limits to the source counts, Col. 9 the exposure time, and Col. 10 the X-ray luminosity. We have used the mean value of the $CECF$ for the compilation of an upper limit to $L_{\mathrm{x}}$ in the case of non-detections. The X-ray luminosity was divided by the number of stellar components.

Multiple stellar systems are represented by a single entry in Tables 2–7, but the designations and if known the spectral types of all components are given. Whenever more than one star lies in the X-ray-to-optical identification radius we list the designations of all possible counterparts.

If a star was detected in both unmerged and merged observations we list only the result from the merged observations. The same applies to stars which are detected

**Table 8.** X-ray statistics of TTS, Pleiads, and Hyads observed and detected in pointed *ROSAT* PSPC observations. $N_{\rm D}$ – Number of detections, $N_{\rm N}$ – Number of non-detections, $N_{\rm stars}$ – Number of different stars observed, $N_{\rm mult.FOV}$ – Number of stars in the FOV of more than one observation, $N_{\rm mult.D}$ – Number of stars detected in more than one observation.

| Sp.Type | $N_{\rm D}$ | $N_{\rm N}$ | $N_{\rm stars}$ | $N_{\rm mult.FOV}$ | $N_{\rm mult.D}$ |
|---|---|---|---|---|---|
| **Taurus-Auriga TTS** | | | | | |
| G | 28 | 19 | 17 | 12 | 11 |
| K | 66 | 30 | 59 | 23 | 19 |
| M | 74 | 88 | 98 | 44 | 33 |
| **Pleiades** | | | | | |
| G | 41 | 82 | 41 | 31 | 20 |
| K | 118 | 231 | 112 | 87 | 59 |
| M | 52 | 139 | 65 | 47 | 31 |
| **Hyades** | | | | | |
| G | 29 | 2 | 22 | 8 | 8 |
| K | 71 | 20 | 54 | 29 | 26 |
| M | 84 | 69 | 99 | 46 | 33 |

neither in the merged nor in the unmerged observations. Here, we list only the upper limit from the merged observation. In a few cases a star was detected in a single but not in the merged observations. This can occur if the source is not within the inner 50′ of the merged observation due to the shift in pointing centers during the merging process, or if the source or background is variable.

Stars which have shown an X-ray flare (discussed by SNH00) are represented by their quiescent emission, i.e. the flare has been removed from the data. We have marked the flare observations in Tables 2–7 by a label after the observation ID.

### 2.4. Detection rates

The aim of this study is to examine the X-ray emission from magnetically active stars. Stars of spectral types earlier than ∼F5 are not expected to show dynamo activity because they have no or only shallow convection zones (Walter 1983). We are not interested in the X-ray emission of these stars because they obey a different emission mechanism. Therefore, we restrict the following analysis to stars with spectral types G and later.

An overview over the detection rates for stars from the different stellar groups is given in Table 8. We have split up each sample according to the spectral types of its members. The column labeled "$N_{\rm D}$" gives the sum of all detections, and "$N_{\rm N}$" is the number of non-detections. The number of observed stars (column $N_{\rm stars}$) is smaller than $N_{\rm D}+N_{\rm N}$ due to multiple observations of a given sky position. The columns labeled "$N_{\rm mult.FOV}$" and "$N_{\rm mult.D}$" denote the total number of stars observed/detected in more than one observation. Note, that for most multiple stars only the spectral type of the primary is known, and therefore the stellar system has only one entry in Table 8.

Histograms of the distribution of spectral types in the different stellar samples are displayed in Fig. 1. We show separate histograms for single and multiple star systems. In the latter sample only the primary is considered. (For most secondaries the spectral type is unknown). The empty histogram bins give the number of stars in the *ROSAT* PSPC field of any observation and the hatched histograms the subgroup of detected stars. The total number of stars displayed in the figure is also given and labeled "$N_{\rm FOV}$" (all observed stars) and "$N_{\rm D}$" (all detected stars) respectively.

As seen in Fig. 1, the detection rate is higher for the Hyades than for the Pleiades or TTS, although the Hyades are older. This is probably due to their shorter distance. The relative number of detections is larger for TTS than for the Pleiades presumably because TTS are young and more active. Throughout all spectral types the detection rate is higher for unresolved binaries as compared to single stars. This could indicate that all stars in multiple systems contribute to the X-ray emission. The actual detection rate is a complicated function of many influencing factors, such as distance, integration time, absorption, age and mass. A detailed analysis of the X-ray emission levels of the different groups of stars is given in the following sections.

### 2.5. X-ray detection of very-late type dwarfs

A number of very low-mass dwarfs with spectral types between M5 and M9 have been detected. In particular, we report on the detection of LH 0429+17, to date the latest PMS dwarf with X-ray emission. This object was listed as a candidate member of the Hyades in a photometric study by Leggett & Hawkins (1989). In the course of a spectroscopic survey for brown dwarfs in the Hyades Reid & Hawley (1999) have detected strong H$\alpha$ emission but weak absorption in the gravity sensitive Na I line, which is an indication for young age. Taking into account its location on the sky, LH 0429+17 can, therefore, be considered as member of the Taurus star forming region.

X-rays from young brown dwarfs and brown dwarf candidates in the Chamaeleon, Taurus-Auriga and $\rho$ Ophiuchus star forming regions have first been observed by Neuhäuser & Comerón (1998) and Neuhäuser et al. (1999). These objects have spectral types between M6 and M8. Note, that we confirm here the detection of all brown dwarfs and brown dwarf candidates in the Taurus region which have been listed in Neuhäuser et al. (1999).

## 3. H-R diagrams

In order to visualize the age and mass distribution of our stars we have placed the subset of TTS observed with the PSPC and with known bolometric luminosity $L_{\rm bol}$ and effective temperature $T_{\rm eff}$ in the Hertzsprung-Russell diagram (H-R diagram). We dispense with H-R diagrams for Pleiades and Hyades stars because most of the stars in these two clusters are well known to lie on the MS (see previous discussion). The H-R diagram for the TTS in Taurus-Auriga is shown in Fig. 2. We have used the

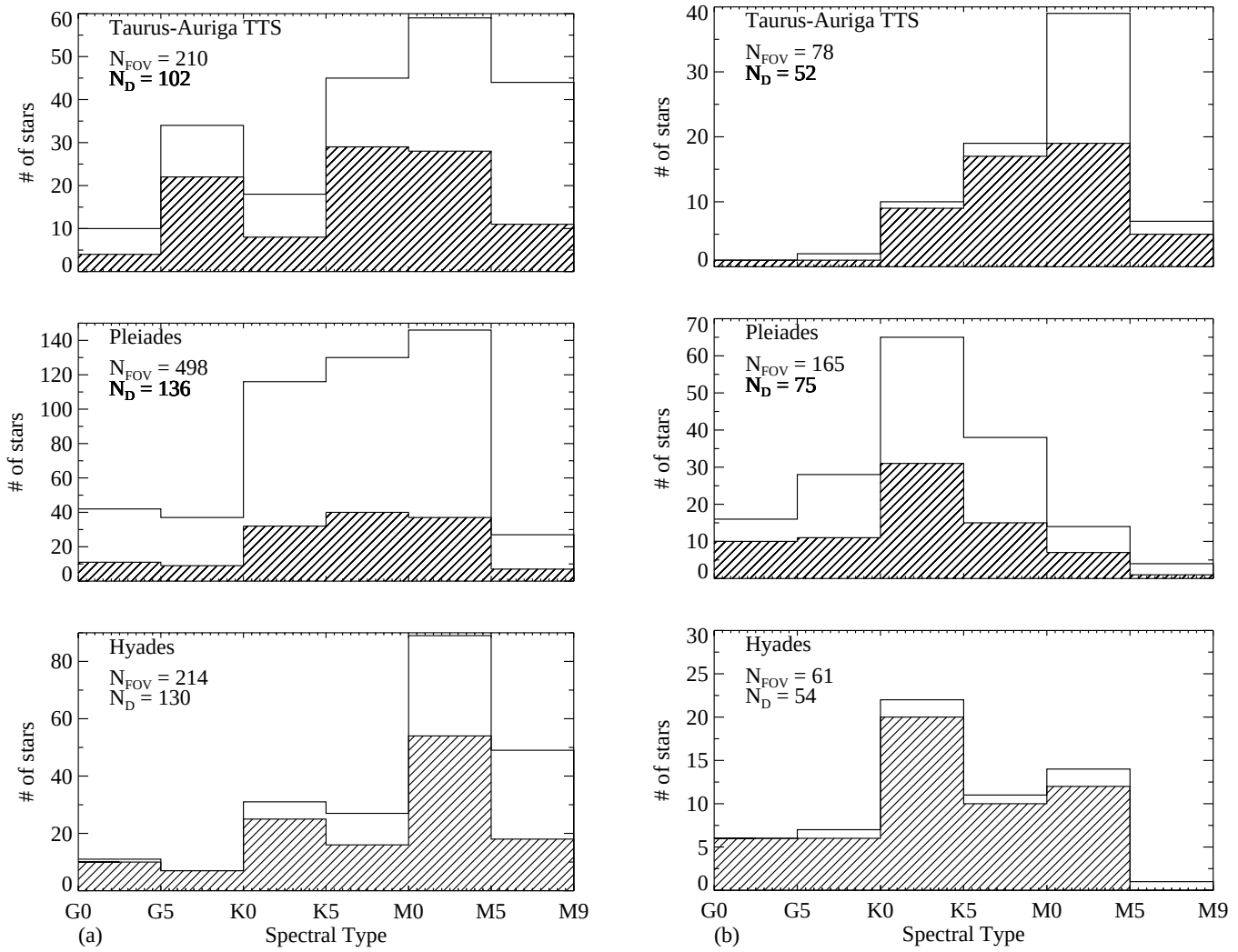


**Fig. 1.** Spectral type distribution of the observed late-type stars: **a)** single stars, **b)** multiple stellar systems. For multiples the spectral type of the primary is plotted, and the secondary is not taken into account. Solid lines denote the total number of stellar systems in any field of the *ROSAT* PSPC observations from Table 1 in SNH00. The hatched areas represent the number of detected systems. The numbers given in each panel represent the total number of observed systems ("$N_{\rm FOV}$") and detected systems ("$N_{\rm D}$"). Note, that individual stellar systems may have been detected in more than one observation. The fraction of detected stars depends on distance, integration time, possible flaring activity, line-of-sight absorption, and stellar parameters such as age, mass, and rotation.

$L_{\rm bol}$ values given by Kenyon & Hartmann (1995), and $T_{\rm eff}$ was obtained from the spectral types using the conversion by Schmidt-Kaler (1982). The location of the stars is compared to different models of evolutionary PMS tracks: D'Antona & Mazzitelli (1994), Baraffe et al. (1998), and Palla & Stahler (1999). All diagrams are drawn with the same scale to facilitate the perception of differences between the model calculations. The computation by Baraffe et al. (1998) does not represent a useful description of the complete TTS sample due to its restriction to masses below $\sim$1 $M_{\odot}$. Furthermore, the lines of equal mass show significant deviations from the other calculations. A closer look reveals that there are also significant differences between the models of D'Antona & Mazzitelli (1994) and Palla & Stahler (1999).

It would be highly desirable to use the theoretical calculations to assign ages and masses to the individual TTS. However, from the comparison provided in Fig. 2 it is obvious that the calibration of the models is uncertain, i.e. tracks computed by different groups would lead to controversial results on the masses and ages of the stars.

Despite such uncertainties the H-R diagram can be used to demonstrate the average distribution of the cTTS and wTTS. Although the stars closest to the birthline tend to be cTTS, and those nearest to the MS are wTTS, the overall distribution of cTTS and wTTS is mixed. This indicates that individual wTTS are not always older than cTTS despite the fact that they represent a later evolutionary stage. This is known since the discovery of many wTTS by the *EO* (Walter et al. 1988), and the situation is similar in other star forming regions.

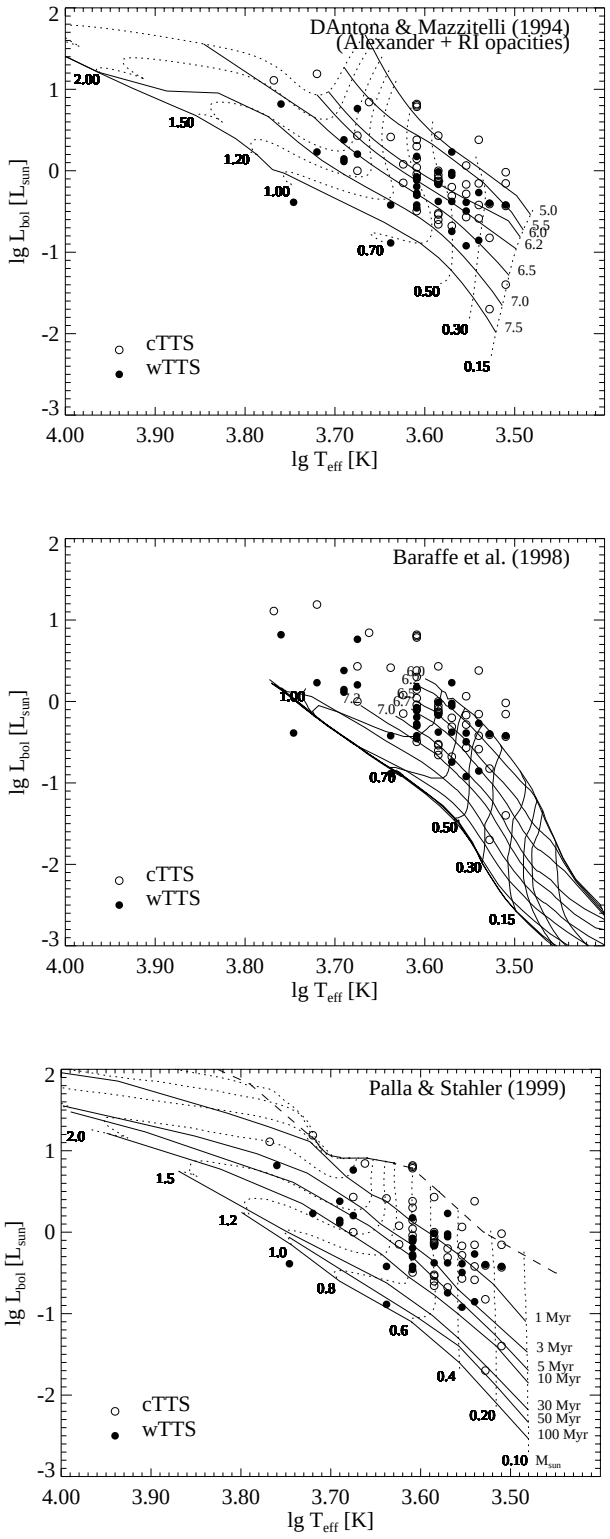


**Fig. 2.** H-R diagram of TTS observed with the *ROSAT* PSPC during pointed observations. Note, that the stars on display represent only a fraction of all X-ray observed TTS because $L_{\rm bol}$ and $T_{\rm eff}$ are not known in all cases. The data are compared to three different theoretical calculations for the PMS evolution: *top* – D'Antona & Mazzitelli (1994), *middle* – Baraffe et al. (1998), and *bottom* – Palla & Stahler (1999). The masses are given in solar units and the isochrones represent log age except for Palla & Stahler (1999) where the ages are given in Myrs.

## 4. X-ray luminosity functions

The statistical analysis was performed with the ASURV package version 1.2 (see Feigelson et al. 1985; Isobe et al. 1986; LaValley et al. 1992). The ASURV software is particularly well suited for the study of data sets with censored points, i.e. non-detections. We exclude photons observed during the large X-ray flares presented by SNH00, i.e. for flaring stars only their quiescent radiation is taken into account.

XLF are frequently employed to characterize a stellar population. Our special interest here is to compare the XLF of the different stellar groups with respect to the following issues: (i) Are the luminosity functions of cTTS and wTTS different, (ii) how does the X-ray luminosity evolve with stellar age, (iii) how does it depend on the spectral types of the stars and their binary character.

A substantial number of stars are in the field of more than one pointed PSPC observation (see Table 8). However, every star should appear only once in the XLF. Therefore, we represent each star by its error weighted mean luminosity from all observations in which it was detected. If a star was observed in more than one observation, but not detected in any of them, we use the mean upper limit of all non-detections of this star as an estimate for its luminosity limit.

In Sect. 4.3 we will justify our assumption that the X-ray luminosity can be distributed equally among all stars in unresolved multiple systems. Therefore, if not specified otherwise, we have divided the mean X-ray luminosity by the number of components in the stellar system.

### 4.1. cTTS and wTTS in RASS and pointed PSPC data

When studying the X-ray emission of TTS in Taurus-Auriga observed during the RASS, N95 found that the wTTS are X-ray brighter than the cTTS. This is in contrast to findings in various other star forming regions (see e.g. Feigelson et al. 1993; Casanova et al. 1995; Grosso et al. 2000). This discrepancy is not yet understood. A possible explanation is that the XLF of the wTTS in Taurus-Auriga is uncomplete towards the low-luminosity end, because wTTS are not easily identified due to the lack of pronounced spectral features. In particular, many wTTS have been discovered with the *EO*. Therefore, even the pre-*ROSAT* sample studied in N95 could be biased towards X-ray bright wTTS.

Our analysis of a large set of pointed *ROSAT* observations allows to extend the sensitivity limit substantially with respect to the RASS. In Fig. 3 we compare the XLF of TTS derived from the pointed observations described in this paper to the results from the RASS. The XLF of the RASS have been newly compiled with respect to the analysis by N95 to include all TTS discovered since then, i.e. the sample consists of all TTS from N95 plus those listed in König et al. (2001) (including both *EO* and *ROSAT* discovered TTS). N95 did include *EO* discovered but no *ROSAT* discovered TTS.

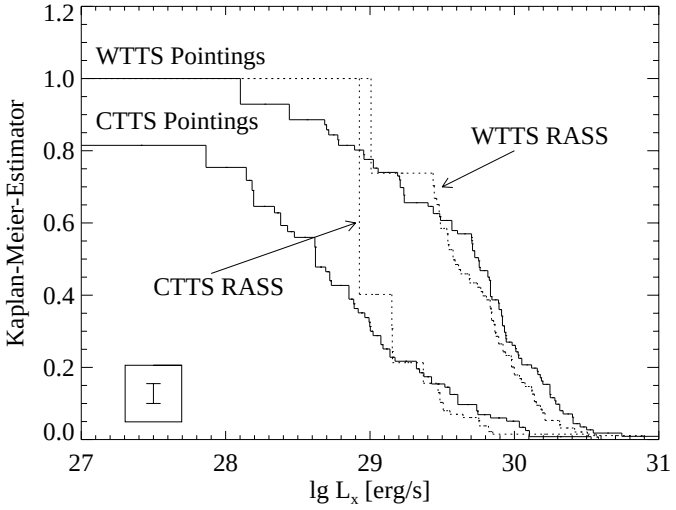


**Fig. 3.** XLF of TTS in Taurus-Auriga derived from the RASS and from pointed *ROSAT* PSPC observations. Shown are all cTTS and wTTS in Taurus-Auriga. The inset in the lower left shows the typical error bar.

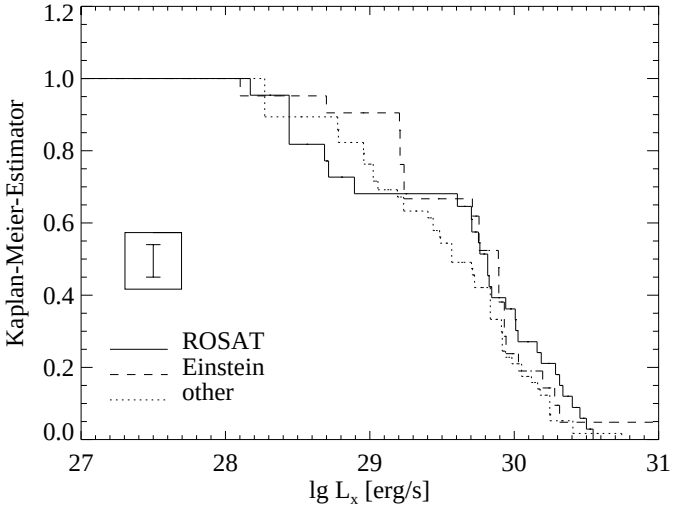


**Fig. 4.** XLF of wTTS in Taurus-Auriga derived from pointed *ROSAT* PSPC observations. The three different distributions are *ROSAT* discovered wTTS (solid line), *EO* discovered wTTS (dashed line), and wTTS discovered by other means (dotted line). The inset in the lower left shows the typical error bar. All distributions are similar indicating that the inclusion of X-ray discovered TTS does not introduce a selection bias into the sample of wTTS.

The comparison with the RASS data clearly demonstrates the better sensitivity of the pointed observations. The XLF computed from the PSPC pointings extends by $\sim$1−2 orders of magnitude further into the low luminosity regime. We reproduce the result first found by N95: in Taurus-Auriga the wTTS are clearly X-ray brighter than the cTTS.

It was noted by Feigelson et al. (1993) that the XLF can change, if the stars included in the sample were found by different methods, e.g. H$\alpha$ versus X-ray surveys. In order to overcome this bias we have computed XLF where we exclude all X-ray discovered TTS. Figure 4 shows the Kaplan-Meier Estimator (KME) for three subsets of wTTS in Taurus-Auriga: *ROSAT* discovered wTTS, *EO* discovered wTTS, and all other wTTS. The XLF of these groups do not differ significantly from each other. Therefore, we are led to conclude that the difference in the distributions of cTTS and wTTS is not due to an X-ray selection bias.

The differences to the $\rho$ Oph and Cha I star forming regions (Feigelson et al. 1993; Casanova et al. 1995; Grosso et al. 2000) could also be caused by the difference in spatial extension between these two young clusters and the Taurus-Auriga region: The latter is widely dispersed, and, hence, its members may constitute a larger spread in age as compared to the more complex $\rho$ Oph and Cha I regions in which the stars are probably more coeval. We can check this by selecting TTS from the central parts of the star forming region, and comparing the resulting XLF with that of the total sample. We have chosen the PSPC observations ROR 200001-0p and 200001-1p pointed on the L1495E cloud. These pointings are centered on the largest concentration of molecular material corresponding to a particular young part of the Taurus complex. In Fig. 5 we show the XLF for wTTS and cTTS in that region. A third distribution consists of all wTTS in L1495E which have *not* been discovered by *ROSAT*. The general shape of the XLF in L1495E is the same as that for the complete Taurus-Auriga area: wTTS are X-ray brighter than cTTS. This is also evident from the data in Strom & Strom (1994), an earlier analysis of these pointings in L1495E. We conclude that the X-ray luminosity does not depend on the spatial location within the Taurus region.

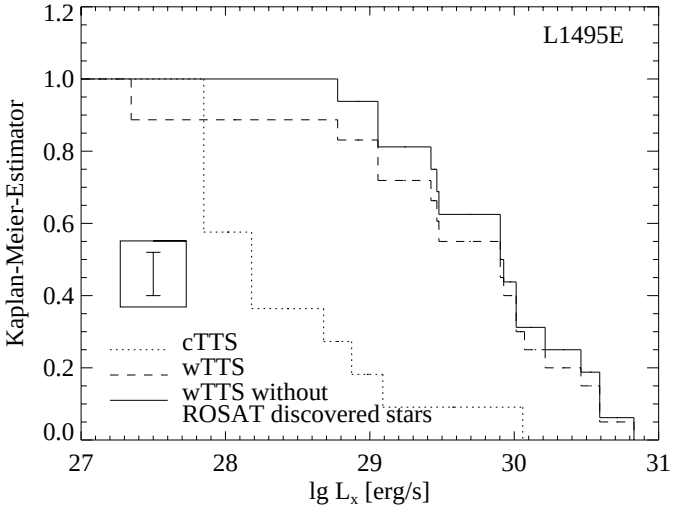


**Fig. 5.** XLF of wTTS and cTTS in L1495E derived from a $\sim$30 ksec pointed *ROSAT* PSPC observation: *dotted line* – cTTS; *dashed line* – all wTTS; *solid line* – wTTS except those discovered by *ROSAT*. The inset in the lower left shows the typical error bar. The distributions of cTTS and wTTS are again different indicating that the discrepancy between the X-ray luminosities of cTTS and wTTS in Taurus-Auriga is not due to the spatial extension of the sample.

The difference in the XLF of wTTS and cTTS does also not depend on our choice of roughly 10 Å as boundary between cTTS and wTTS. It is clear that one should use the H$\alpha$ flux instead of the equivalent width as boundary (hence, we classify SU Aur as cTTS) because the equivalent width depends on the underlying continuum which varies with spectral type. Martín (1997) suggested three different equivalent width boundaries for three spectral type regimes chosen such as to exclude that the H$\alpha$ emission is due to chromospheric activity. Adopting these criteria only a few TTS change classification, but the difference in the XLF remains.

In Sect. 2.3 the conversion from count rates to luminosities by use of hardness ratios was explained. Using hardness ratios allows to indirectly take account of the extinction in the absence of actual $A_V$ measurements. However, $HR1$ is only sensitive to comparatively low extinctions. The extinction should generally be higher for the cTTS than for the wTTS due to the denser circumstellar environment of the former ones, and if not treated properly may lead to wrong estimates for the luminosities.

We have, therefore, applied an alternative way of deriving X-ray luminosities for the TTS in Taurus-Auriga making use of the available $A_V$ data. In this approach the X-ray flux was computed with standard EXSAS tools assuming a 1 keV RS-model with absorbing column density $N_{\rm H}$ derived from $A_V$ according to Paresce (1984). Similar values for $N_{\rm H}$ are obtained when using the conversion given by Ryter (1996). Stars for which $A_V$ is $\leq$0.05 mag have been assigned a standard value of $N_{\rm H} = 10^{18}$ cm$^{-2}$.

While for individual stars the $L_{\rm x}$ derived by the two methods show typical deviations of $\sim$50%, the statistical distribution of X-ray luminosities is unaffected by the specific choice of $CECF$, and the previously discussed differences between the XLF of cTTS and wTTS remain.

### 4.2. Dependence on spectral type

In the previous subsection, no distinction was drawn between stars of different spectral type, mass or other stellar parameters. This is justified for young, very low-mass stars which follow fully convective tracks. It is believed that for stars on the MS activity is governed by the relative size of radiative core and convective envelope. This should also apply to TTS once they have reached the radiative part of their PMS evolution. Therefore, to obtain homogeneous samples, stars with different interior structure, i.e. different mass, should be treated separately. As argued in Sect. 3 it is not possible to obtain reliable values for the individual masses and ages of the stars. As an approximation we distinguish the stars by their spectral type. But note, that while for stars on their Hayashi tracks this description is acceptable, for stars on radiative tracks a given spectral type represents a mass range rather than a single value for the mass.

Each subsample is subdivided in three spectral type bins: G, K, and M stars. The mean X-ray luminosities for the different stellar groups and spectral types are listed in Table 9. For all spectral types the wTTS distribution shows the largest values of $\langle \log L_{\rm x} \rangle$, and the Hyades have the lowest $\langle \log L_{\rm x} \rangle$. Note, that the group of cTTS of spectral type G is represented by only two stars. But for the other subsamples the statistics are significant. Since in most cases the spectral type (or $B-V$) is known only for the primary in multiples, we exclude the secondaries from this part of the analysis, except the few cases where the spectral types of all components are known (see Tables 2–7).

In Fig. 6 we provide a comparison of the XLF of TTS, Pleiads, and Hyads. Throughout all examined spectral types the wTTS clearly represent the brightest class among the X-ray objects studied here, and Hyads show the weakest X-ray emission. For the M stars, where the mass range is comparatively small, the decline of $L_{\rm x}$ from TTS over Pleiades to the Hyades can be interpreted as an age effect. G and K type stars represent a larger spread in the mass distribution such that the influences of mass and age may not easily be disentangled. However, the difference between $\langle L_{\rm x} \rangle$ of Pleiades and Hyades decreases towards earlier types indicating that age and not mass is the dominant effect.

The distributions of cTTS and Pleiads intersect each other because of the much shallower slope of the XLF of cTTS, i.e. larger spread in luminosities. This effect may be caused by our assumption of uniform distance for all stars in a given sample: in contrast to the strongly clustered Pleiades region the TTS in Taurus-Auriga may be subject to a larger distance spread that translates to an apparent spread in $L_{\rm x}$.

Luminosity differences between various stars may generally be due to differences in emitting area. In order to eliminate this effect the X-ray to bolometric luminosity ratio, $\log(L_{\rm x}/L_{\rm bol})$, is often used to characterize the X-ray emission. We have examined the relation between the effective temperature and $\log(L_{\rm x}/L_{\rm bol})$. $L_{\rm bol}$ of Pleiads and Hyads was computed from the $V$ magnitude and $B-V$ (needed to determine the bolometric correction) given in the Open Cluster Data Base. The effective temperatures of Pleiades and Hyades stars were obtained from $B-V$. We have assumed negligible absorption to both star clusters. In Fig. 7 all late-type stars (spectral type later than F or $\log T_{\rm eff} < 3.78$) are plotted. Figure 7 shows that within the TTS sample, which is characterized by a decline of $\log L_{\rm x}$ with spectral type, $\log(L_{\rm x}/L_{\rm bol})$ does not depend on effective temperature. Pleiades and Hyades, however, demonstrate a clear anticorrelation between $\log(L_{\rm x}/L_{\rm bol})$ and $\log T_{\rm eff}$ (see also e.g. Micela et al. 1999). The fact that we do not see such a trend in the TTS sample may be due to the large age spread among the TTS. Note, that in Fig. 7 only stars with known projected rotational velocity are shown. The plotting symbols have been scaled to $v \sin i$. With few exceptions the fastest rotators are situated close to the upper envelope, indicating a connection between the activity level and the rotation rate (see also Sect. 5).

**Table 9.** Mean X-ray luminosities $\langle \log L_x \rangle$ for cTTS, wTTS, and Pleiades and Hyades. The columns labeled "$N$" and "$N_{lim}$" give the number of stars and number of upper limits within the sample. The second column provides a description of the sample: "C" – cTTS, "W" – wTTS, "s" – single star, "b1" – binary star assuming that all X-ray emission comes from one component, "b2" – binary star assuming equal X-ray emission from both components.

| Region | | Spectral Type G | | | Spectral Type K | | | Spectral Type M | | |
|---|---|---|---|---|---|---|---|---|---|---|
| | | $N$ | $N_{lim}$ | $\log L_x$ | $N$ | $N_{lim}$ | $\log L_x$ | $N$ | $N_{lim}$ | $\log L_x$ |
| TTS | C | 2 | (1) | $29.60 \pm 0.66$ | 22 | (9) | $28.93 \pm 0.16$ | 61 | (30) | $28.54 \pm 0.14$ |
| TTS | W | 15 | (0) | $30.02 \pm 0.17$ | 36 | (5) | $29.78 \pm 0.10$ | 34 | (9) | $29.20 \pm 0.10$ |
| Pleiades | | 41 | (18) | $28.98 \pm 0.12$ | 112 | (41) | $28.94 \pm 0.06$ | 65 | (29) | $28.80 \pm 0.07$ |
| Hyades | | 22 | (2) | $28.97 \pm 0.05$ | 54 | (6) | $28.52 \pm 0.11$ | 99 | (38) | $27.99 \pm 0.10$ |
| TTS | s | - | - | - | 34 | (11) | $29.44 \pm 0.14$ | 60 | (28) | $28.70 \pm 0.14$ |
| TTS | b2 | - | - | - | 17 | (3) | $29.47 \pm 0.18$ | 29 | (20) | $28.85 \pm 0.18$ |
| TTS | b1 | - | - | - | 17 | (3) | $29.77 \pm 0.18$ | 29 | (10) | $29.15 \pm 0.18$ |
| Pleiades | s | 25 | (13) | $28.98 \pm 0.15$ | 84 | (38) | $28.83 \pm 0.09$ | 60 | (29) | $28.78 \pm 0.08$ |
| Pleiades | b2 | 16 | (5) | $29.03 \pm 0.16$ | 27 | (3) | $29.00 \pm 0.08$ | 5 | (0) | $28.93 \pm 0.08$ |
| Pleiades | b1 | 16 | (5) | $29.33 \pm 0.16$ | 27 | (3) | $29.30 \pm 0.08$ | 5 | (0) | $29.23 \pm 0.08$ |
| Hyades | s | 12 | (1) | $28.97 \pm 0.06$ | 36 | (5) | $28.41 \pm 0.15$ | 89 | (35) | $27.95 \pm 0.10$ |
| Hyades | b2 | 10 | (1) | $28.96 \pm 0.07$ | 18 | (1) | $28.75 \pm 0.14$ | 9 | (3) | $28.47 \pm 0.19$ |
| Hyades | b1 | 10 | (1) | $29.26 \pm 0.07$ | 18 | (1) | $29.05 \pm 0.14$ | 9 | (3) | $28.77 \pm 0.19$ |

### *4.3. Single and binary stars*

All XLF presented above may rely to some degree on our assumption that all components in multiple systems emit X-rays (at the same level). In order to check this hypothesis we have studied the XLF of single and binary stars separately. Again we have constructed separate XLF for G, K, and M type stars. In Fig. 8 we show these XLF for TTS, Pleiades and Hyades stars. For comparison we display also the XLF for binaries derived without taking account of the binary character, i.e. XLF in which each binary has been regarded as a single star with the observed X-ray luminosity (dashed in Fig. 8). Henceforth, these distributions are termed "b1", in contrast to the distributions "b2" for which equal partition of $L_x$ onto the components was assumed (dotted in Fig. 8). As before, binary components with unknown spectral type are not considered.

The mean and median of $\log L_x$ for all compiled distributions are listed in Table 9. Obviously, throughout all examined groups of stars the distributions "b1" are shifted towards higher luminosities with respect to the distributions "b2". We have performed two-sample tests within ASURV to quantify the differences. The results are summarized in Table 10. The comparison between "s" and "b2" shows in most cases a high probability that the distributions are similar. Only for the Hyades K and M stars the probability that the distributions of singles and "b2" are different is ∼90%. All samples "s" and "b1", on the contrary, have high probability for different underlying parent distributions.

The XLF of Hyades stars have first been examined by Pye et al. (1994) on the basis of *ROSAT* observations. Their finding that Hyades dK binaries are X-ray brighter than single Hyads of the same spectral type were confirmed by Stern et al. (1995) on a larger sample. Our analysis shows that the comparison depends sensitively on the way in which binary stars are treated. The effect is strongly reduced if it is assumed that both components in

**Table 10.** Results of two-sample tests performed with ASURV to distinguish between the XLF of single and binary stars. For each group (TTS, Pleiads, and Hyads) and each spectral type we have compared three distributions: s – single stars, b1 – binary stars with only one X-ray emitter, b2 – binary stars assuming that both components emit equal amounts of X-rays. The probabilities given are for the null-hypothesis that the compared pair of XLF is drawn from the same parent distribution. We have applied Gehan's generalized Wilcoxon test (GW), the logrank test, and the Peto & Prentice generalized Wilcoxon test.

| Sample | size (ul.) | Prob GW HV | Prob log rank | Prob P & Pren. |
|---|---|---|---|---|
| **TTS K stars** | | | | |
| s-b2 | 34 (11)–17 (3) | 0.948 | 0.852 | 0.948 |
| s-b1 | 34 (11)–17 (3) | 0.073 | 0.165 | 0.084 |
| **TTS M stars** | | | | |
| s-b2 | 60 (28)–29 (10) | 0.238 | 0.471 | 0.275 |
| s-b1 | 60 (28)–29 (10) | 0.006 | 0.051 | 0.010 |
| **Pleiads G stars** | | | | |
| s-b2 | 25 (13)–16 (5) | 0.844 | 0.953 | 0.789 |
| s-b1 | 25 (13)–16 (5) | 0.085 | 0.103 | 0.089 |
| **Pleiads K stars** | | | | |
| s-b2 | 84 (38)–27 (3) | 0.825 | 0.286 | 0.688 |
| s-b1 | 84 (38)–27 (3) | 0.002 | 0.001 | 0.004 |
| **Pleiads M stars** | | | | |
| s-b2 | 60 (29)–5 (0) | 0.710 | 0.294 | 0.665 |
| s-b1 | 60 (29)–5 (0) | 0.002 | 0.001 | 0.009 |
| **Hyads G stars** | | | | |
| s-b2 | 12 (1)–10 (1) | 0.657 | 0.711 | 0.620 |
| s-b1 | 12 (1)–10 (1) | 0.003 | 0.005 | 0.005 |
| **Hyads K stars** | | | | |
| s-b2 | 36 (5)–18 (1) | 0.134 | 0.095 | 0.150 |
| s-b1 | 36 (5)–18 (1) | 0.000 | 0.000 | 0.001 |
| **Hyads M stars** | | | | |
| s-b2 | 89 (35)–9 (3) | 0.059 | 0.217 | 0.083 |
| s-b1 | 89 (35)–9 (3) | 0.002 | 0.022 | 0.005 |

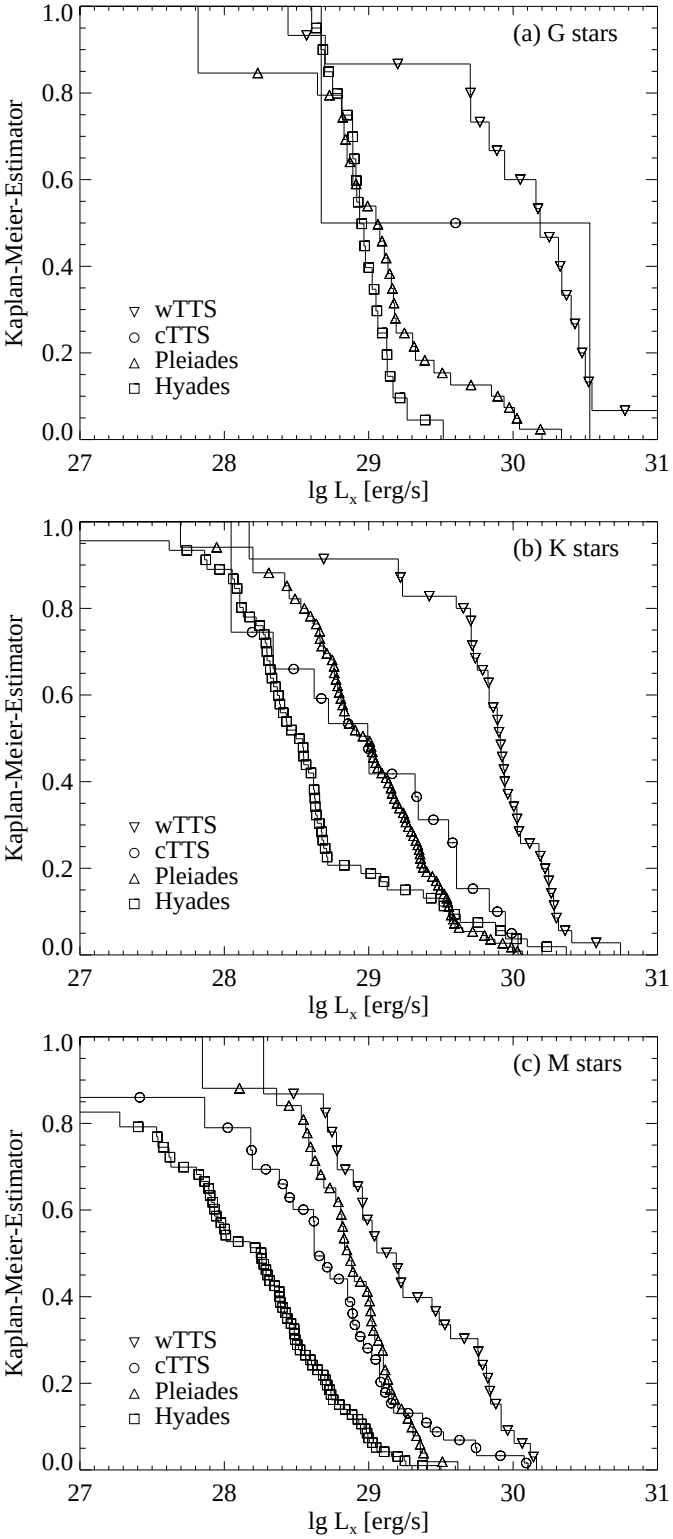


**Fig. 6.** XLF for TTS in Taurus-Auriga, for the Pleiades, and the Hyades. The distributions are shown for different spectral types, corresponding to different values of $B-V$ or effective temperature or mass for the MS stars. **a)** G stars, **b)** K stars, and **c)** M stars.

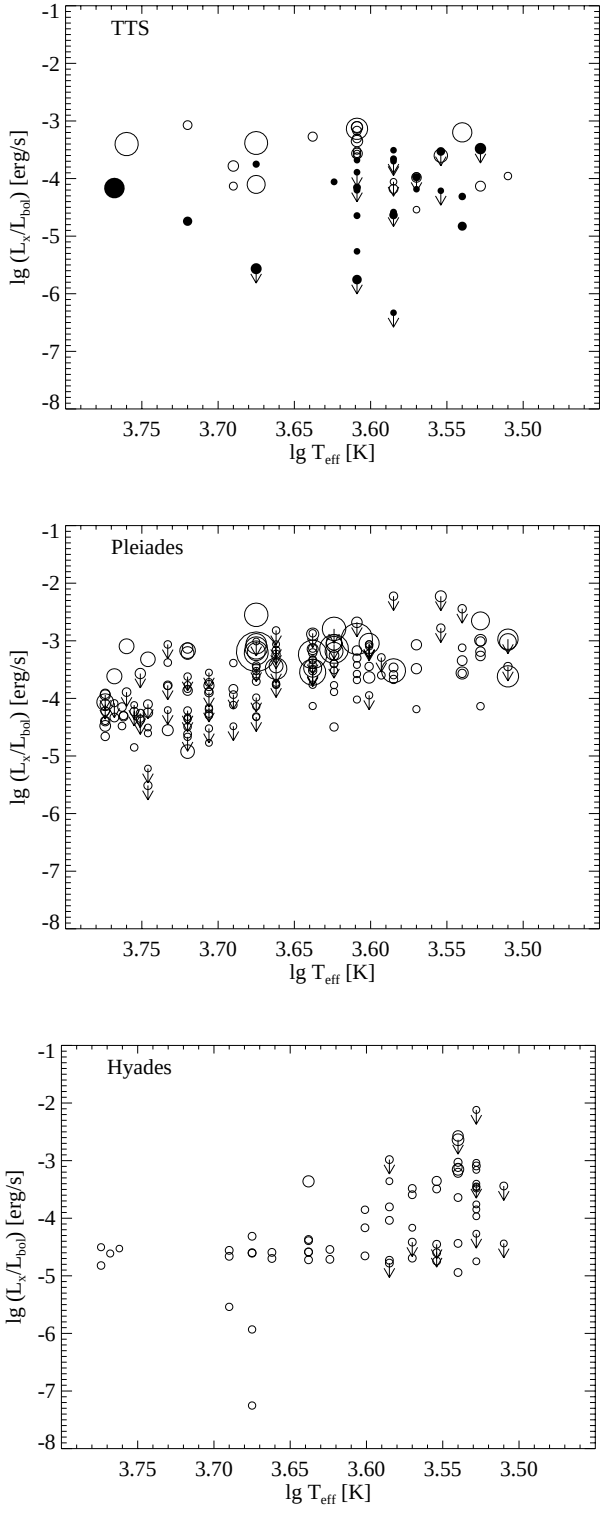


**Fig. 7.** Relation between X-ray to bolometric luminosity ratio, $\log(L_{\rm x}/L_{\rm bol})$, and effective temperature, $\log T_{\rm eff}$. From top to bottom: TTS, Pleiades, and Hyades. Only stars with spectral type later than F are considered. The plotting symbols have been scaled to the projected rotational velocity of the stars. Upper limits to $L_{\rm x}$ are indicated by arrows.

binaries emit X-rays ("b2") with respect to distributions of type "b1" examined by Pye et al. (1994) and Stern et al. (1995).

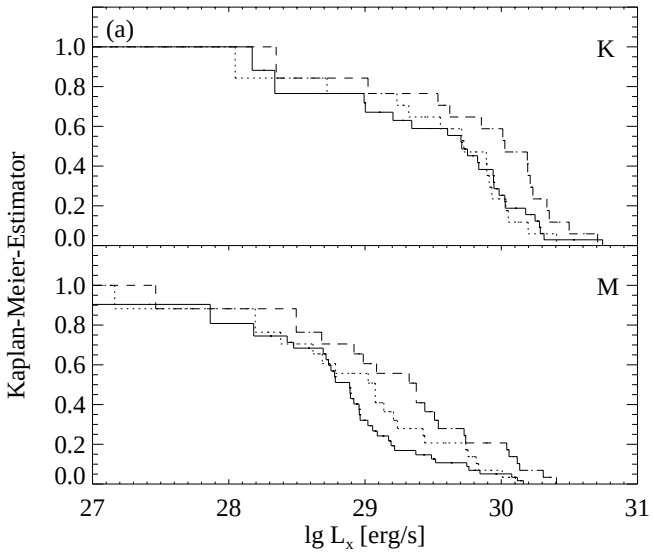


**Fig. 8.** XLF of single and binary stars of spectral type G, K and M. **a)** TTS, **b)** Pleiades, and **c)** Hyades. *solid lines* – single stars (s), *dotted lines* – binary stars assuming equal $L_x$ from both components (b2), *dashed lines* – binary stars assuming only one X-ray emitting component (b1). See text for a more detailed description of these samples. All G type TTS in Taurus-Auriga are single stars, and therefore not displayed in this figure.

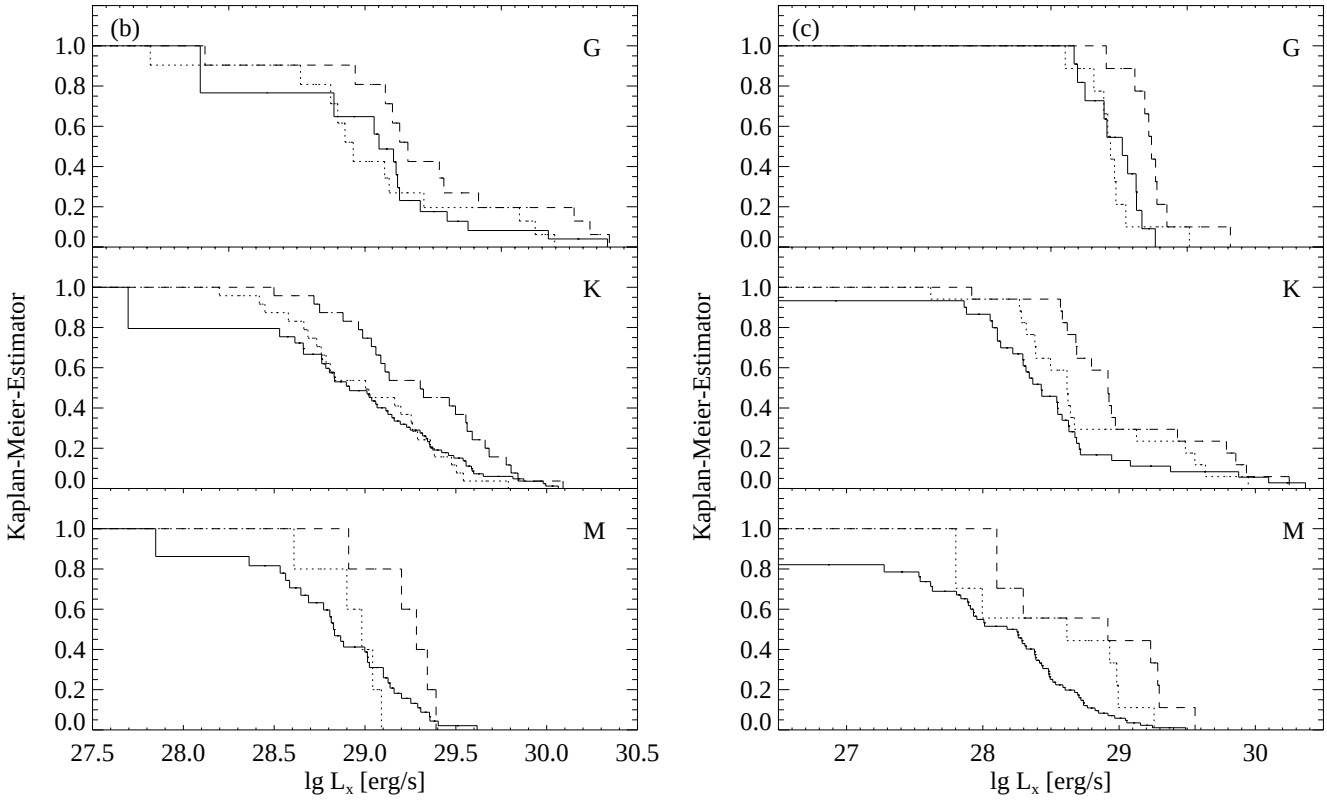


## 5. Rotation-activity relations

The rotation-activity connection has been extensively studied by Walter (1981), Walter & Bowyer (1981), Walter (1982), Bouvier (1990), Damiani et al. (1991), Grankin (1993), N95, Bouvier et al. (1997b), and Wichmann et al. (1998a).

In this section we study the subsample of the stars from Tables 2 to 7 with measured rotation periods $P_{\rm rot}$ or projected rotational velocity $v \sin i$. The choice of the best parameters describing the activity-rotation relation is not undisputed. We have, therefore, examined different parameter combinations. On the X-ray side we use the luminosity $L_{\rm x}$, the surface flux $F_{\rm s}$, and the ratio between X-ray and bolometric luminosity $L_{\rm x}/L_{\rm bol}$ to characterize the stars. Each star is represented by its mean X-ray luminosity or upper limit to $L_{\rm x}$ as described in Sect. 4. For binaries only one component is considered, because spectral types and rotation rates are in most cases known only for the primary. The stellar radii used to compute $F_{\rm s}$ were determined from the Stefan-Boltzmann law. The rotation is described by the projected rotational velocity, $v \sin i$, or

the rotation period, $P_{\rm rot}$. $P_{\rm rot}$ and $v \sin i$ of Pleiades and Hyades stars are listed in the Open Cluster Data Base. Values for the rotation rates of TTS are taken from N95, Bouvier et al. (1997b), and Wichmann et al. (1998a).

For the statistical analysis cTTS and wTTS have been combined to yield a larger sample, although generally wTTS are faster rotators than cTTS, and they are more X-ray luminous. A linear regression has been fitted to all pairs of rotation-activity combinations using the ASURV EM algorithm or the method by Schmitt (1985) for doubly censored data. In Table 11 we summarize the results of all correlation tests, and also give the slopes of the linear regression. According to the statistical tests X-ray emission and rotation are clearly correlated for most of the examined stellar samples. For a given X-ray parameter the probability for a correlation with $P_{\rm rot}$ is in most cases larger than the probability for a correlation with $v \sin i$. This is probably due to the unknown inclination angle in $v \sin i$ whose arbitrary orientation tends to destroy any intrinsic correlation between the rotation and X-ray emission. Using $P_{\rm rot}$ should therefore be more meaningful. However, measurements of the actual periods (by spot modulation) are much sparser than spectroscopic observations of $v \sin i$, leading to a smaller data set.

We show correlations of all possible combinations of the above mentioned X-ray parameters with $P_{\rm rot}$ in Figs. 9 to 11 for TTS, Pleiads, and Hyads. Overlaid are the linear regressions corresponding to the power law relation from Table 11. The lowest significance is found in the Hyades. This may however be due to the limited range in rotation period (only two stars with $P_{\rm rot} < 4$ d), and because the Hyades with known period have a small range of spectral types.

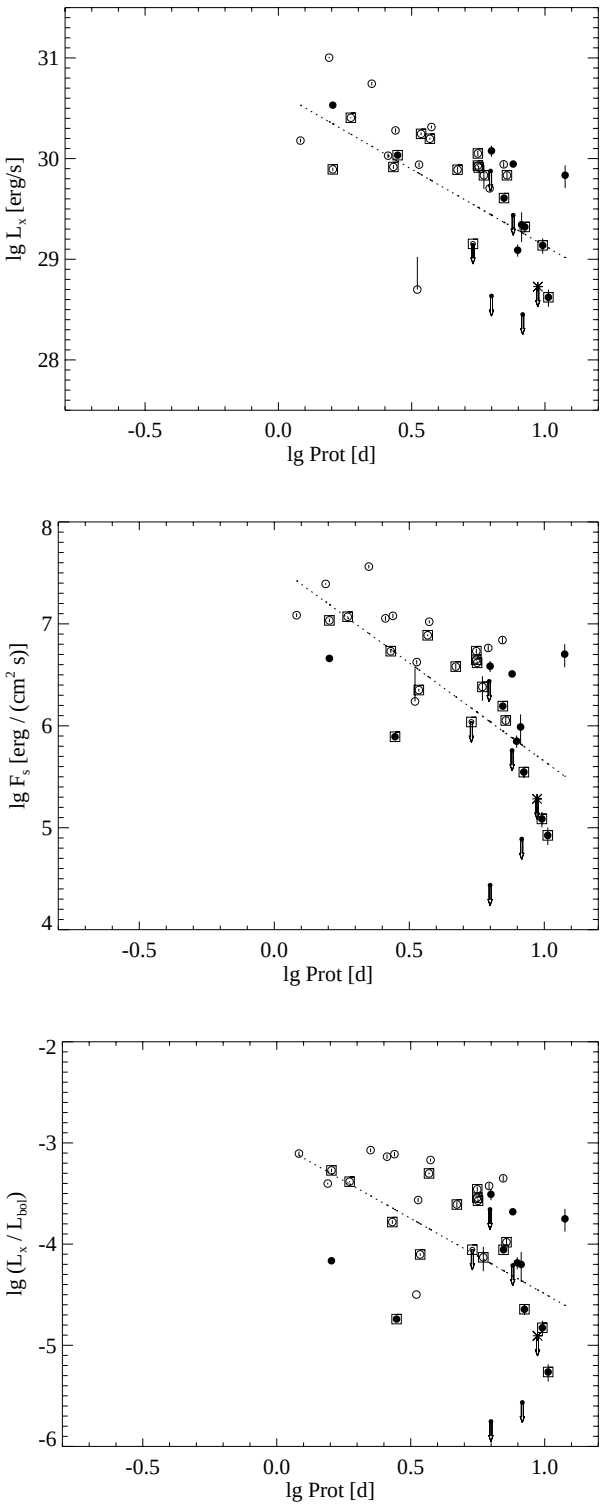


**Fig. 9.** Relation between the rotation period and different X-ray parameters for TTS from the Taurus-Auriga region: *top* – X-ray luminosity, *middle* – X-ray surface flux, and *bottom* – Ratio between X-ray luminosity and bolometric luminosity. cTTS are represented by filled symbols and wTTS by open symbols. TTS of unknown nature are displayed as asterisks. Multiple stars are marked by boxes. The solid lines are linear regressions computed with the EM algorithm implemented in ASURV. The size of the errors bars varies a lot due to very different *ROSAT* exposure times, and they are sometimes smaller than the plotting symbol.

## 6. Discussion

### 6.1. The XLF of cTTS and wTTS

We have reanalysed the XLF for cTTS and wTTS in Taurus-Auriga, first presented by N95, increasing the sensitivity with respect to the RASS by ∼2 orders of magnitude. Our pointed PSPC observations confirm that in Taurus-Auriga wTTS are on average more X-ray luminous than cTTS. This is in contrast to studies of Cha I and $\rho$ Oph (Feigelson et al. 1993; Casanova et al. 1995; Grosso et al. 2000), where no difference was found between the two sub-classes of TTS concerning their X-ray emission level. In a study of the Orion Nebula region with the *ROSAT* HRI Gagné & Caillault (1995) found slightly lower median $L_{\rm x}$ and $L_{\rm x}/L_{\rm bol}$ values for stars with massive accretion disks, i.e. cTTS. Alcalá et al. (1997) have found higher X-ray luminosities for *ROSAT* discovered wTTS in the outer parts of the Cha I and Cha II regions. This seems to indicate that samples of wTTS may be biased towards strong X-ray emitters, and that discrepancies can arise from the different spatial distribution of the cTTS and wTTS sample.

**Table 11.** Results of statistical tests with ASURV for the relation between X-ray emission and stellar rotation for TTS, Pleiads, and Hyads. The first two columns are the names of the two parameters to be compared. Next is the size of the sample, $N$, and in brackets the number of upper limits, $N_{\rm lim}$, to the rotation and X-ray parameter. Columns 5 and 6 give the probability that there is *no* correlation between the two parameters according to Kendall's and Spearman's test. The slope of a linear regression to the pair of parameters is given in Col. 7. For doubly censored data we have used the linear regression method of Schmitt (1985). All samples where $P_{\rm rot}$ is the rotation parameter have upper limits only in the X-ray parameters, and the EM algorithm is used.

| Par 1 | Par 2 | $N$ | $N_{\rm lim}$ | Kendall | Spearman | slope |
|---|---|---|---|---|---|---|
| | | | **TTS** | | | |
| $\log(v \sin i)$ | $\log L_{\rm x}$ | 65 | (0/17) | 0.0031 | 0.0047 | $1.08 \pm 0.36$ |
| $\log(v \sin i)$ | $\log F_{\rm s}$ | 52 | (0/14) | 0.0009 | 0.0011 | $1.57 \pm 0.46$ |
| $\log(v \sin i)$ | $\log(L_{\rm x}/L_{\rm bol})$ | 52 | (0/14) | 0.0053 | 0.0040 | $1.22 \pm 0.44$ |
| $\log P_{\rm rot}$ | $\log L_{\rm x}$ | 39 | (0/7) | 0.0000 | 0.0001 | $-1.52 \pm 0.39$ |
| $\log P_{\rm rot}$ | $\log F_{\rm s}$ | 38 | (0/6) | 0.0000 | 0.0000 | $-1.93 \pm 0.39$ |
| $\log P_{\rm rot}$ | $\log(L_{\rm x}/L_{\rm bol})$ | 38 | (0/6) | 0.0001 | 0.0002 | $-1.49 \pm 0.42$ |
| | | | **Pleiades** | | | |
| $\log(v \sin i)$ | $\log L_{\rm x}$ | 164 | (6/53) | 0.0000 | 0.0000 | 0.61 |
| $\log(v \sin i)$ | $\log F_{\rm s}$ | 164 | (6/53) | 0.0000 | 0.0000 | 0.67 |
| $\log(v \sin i)$ | $\log(L_{\rm x}/L_{\rm bol})$ | 164 | (6/53) | 0.0000 | 0.0000 | 0.88 |
| $\log P_{\rm rot}$ | $\log L_{\rm x}$ | 46 | (0/13) | 0.0008 | 0.0005 | $-0.42 \pm 0.11$ |
| $\log P_{\rm rot}$ | $\log F_{\rm s}$ | 46 | (0/13) | 0.0000 | 0.0001 | $-0.52 \pm 0.11$ |
| $\log P_{\rm rot}$ | $\log(L_{\rm x}/L_{\rm bol})$ | 46 | (0/13) | 0.0000 | 0.0000 | $-0.66 \pm 0.12$ |
| | | | **Hyades** | | | |
| $\log(v \sin i)$ | $\log L_{\rm x}$ | 67 | (41/2) | 0.0008 | 0.0000 | 1.58 |
| $\log(v \sin i)$ | $\log F_{\rm s}$ | 67 | (41/2) | 0.0000 | 0.0001 | 1.56 |
| $\log(v \sin i)$ | $\log(L_{\rm x}/L_{\rm bol})$ | 67 | (41/2) | 0.0003 | 0.0089 | 1.64 |
| $\log P_{\rm rot}$ | $\log L_{\rm x}$ | 21 | (0/2) | 0.0003 | 0.0004 | $-1.13 \pm 0.32$ |
| $\log P_{\rm rot}$ | $\log F_{\rm s}$ | 21 | (0/2) | 0.0016 | 0.0016 | $-0.94 \pm 0.28$ |
| $\log P_{\rm rot}$ | $\log(L_{\rm x}/L_{\rm bol})$ | 21 | (0/2) | 0.3515 | 0.3489 | $-1.51 \pm 0.32$ |

We have ruled out such an X-ray selection bias for our sample, by comparing the XLF for wTTS discovered by means of their X-ray emission to those which have been identified in other ways. XLF constructed for a coeval subgroup of cTTS and wTTS located in a central portion of the Taurus-Auriga complex, the L1495E cloud, show the same disagreement. Therefore, the difference does not seem to be related to the wide spatial extension (hence large age spread) of the Taurus star forming region. In addition this test shows that the disagreement is not caused by the different sensitivities (due to different exposure times) of the various combined PSPC observations.

Further effects, like different spectral type distribution, the specific choice of the $W_{\rm H\alpha}$ boundary between cTTS and wTTS, or our way of splitting the X-ray emission on all components in multiples, can not explain the observed discrepancies between the cTTS and wTTS XLF. To investigate whether the high number of upper limits in the cTTS sample affects the shape of the XLF we have also computed XLF neglecting all upper limits. (Grosso et al. 2000 have not included upper limits in their XLF of $\rho$ Oph.) The structure of the XLF, however, remains unaffected.

We conclude that there is an intrinsic difference in X-ray emission from cTTS and wTTS in Taurus. Besides the extinction effect discussed above the different evolutionary state of TTS in different star forming regions may contribute to the observed discrepancies. It should be noted that the subsamples of cTTS and wTTS in Taurus with known $T_{\rm eff}$ and $L_{\rm bol}$ occupy the same region in the H-R diagram, i.e. the difference in $L_{\rm x}$ seems not to be a direct age effect.

The correlation between the X-ray luminosity and $P_{\rm rot}$ we found for all examined samples suggests that the X-ray emission level may be governed by rotation. To check this hypothesis we have computed separate XLF for fast rotating wTTS ($v \sin i > 22$ km s$^{-1}$, the mean $v \sin i$ for wTTS), and slowly rotating wTTS ($v \sin i < 12$ km s$^{-1}$). Indeed, the slow rotators are characterized by lower X-ray luminosity ($\log L_{\rm x,mean} = 29.54 \pm 0.13$ versus $30.00 \pm 0.11$ for the fast group). This explains some but not all of the discrepancy between the XLF of Fig. 3. From the mean rotation rate of cTTS and wTTS and the mean $\log L_{\rm x}$ values derived from the KME analysis the slope in Fig. 9 would be expected to be much steeper. But note, that only a small fraction of TTS has measured rotation periods, and the large spread in the observed rotation-activity relation may be due to mixing of stars with different mass.

If, indeed, rotation is the major parameter that determines the amount of X-rays emitted by a given star then cTTS and wTTS in Taurus-Auriga are expected to have different $L_{\rm x}$ because the wTTS are on average faster rotators (see Bouvier et al. 1993 and our Fig. 9). Different distributions of rotation periods are also found in other star forming regions, e.g. Lupus (Wichmann et al. 1998b). Only in Orion cTTS and wTTS are found to rotate at the

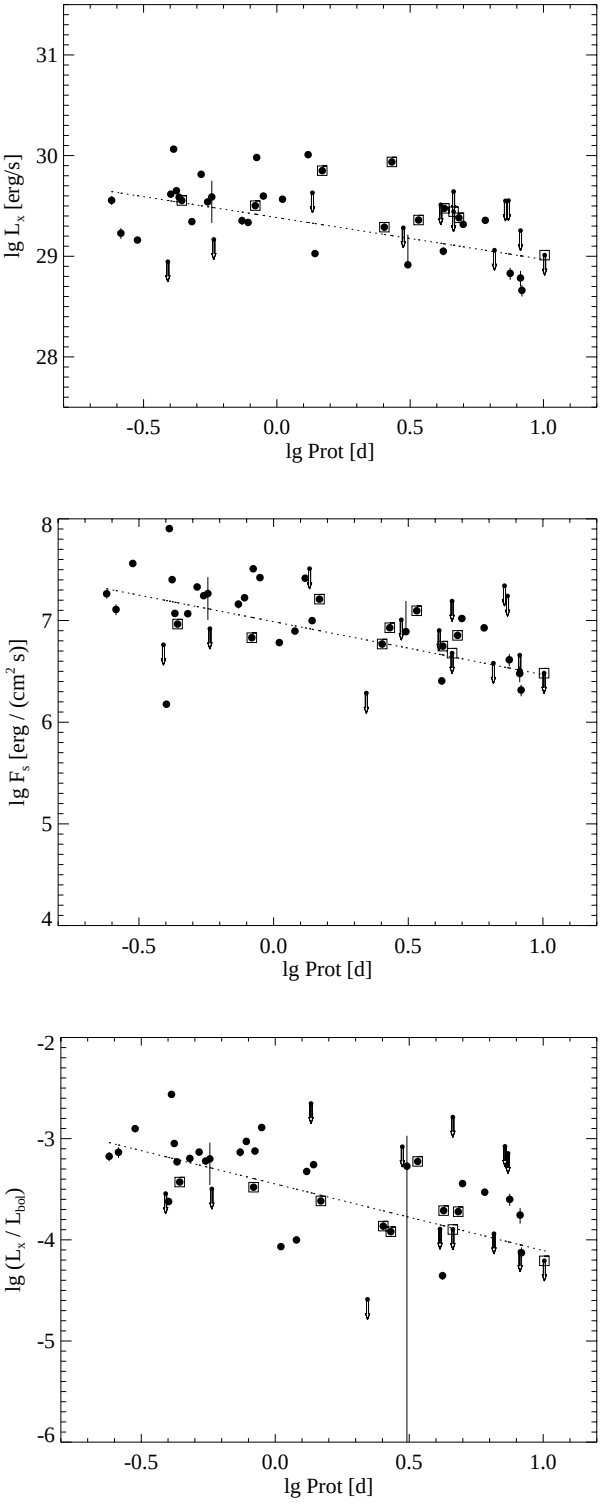


**Fig. 10.** Same as Fig. 9 for the Pleiades.

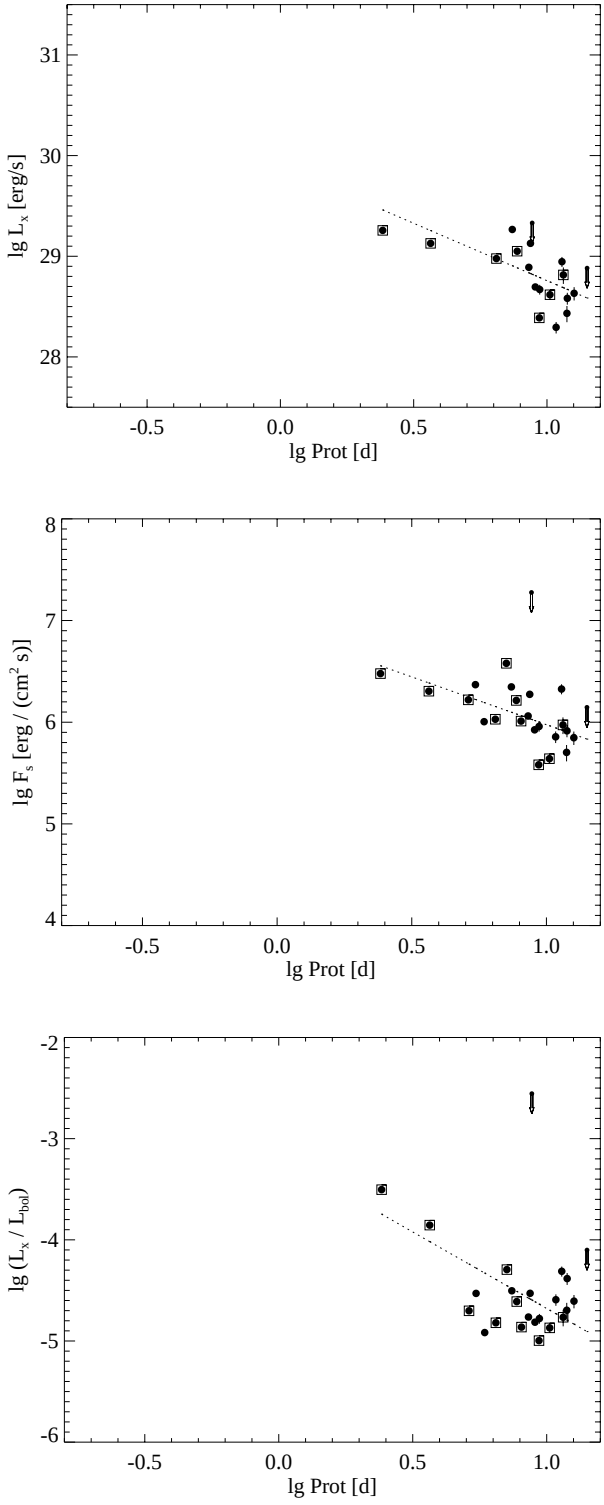


**Fig. 11.** Same as Fig. 9 for the Hyades.

same speed (Stassun et al. 1999). The rotational state of the PMS stars in Cha I and $\rho$ Oph has not yet been investigated in detail. We suspect that most of the wTTS in Taurus-Auriga (including those in L1495E) have spent a longer time than those in Cha I and $\rho$ Oph since they have dispersed their disks, and therefore have had more time to spin up, and consequently should drive a more powerful dynamo. This implies that the disk lifetimes depend on the local condition in the star forming region. We remark that this hypothesis can only be tested after more measurements of rotational velocities in these different regions are available. In a later paper we will compare the XLF in different star forming regions in more detail.

### 6.2. Spectral type and age dependence of the X-ray emission

We have compared the XLF of TTS in Taurus-Auriga, the Pleiades, and the Hyades. Following early studies by the *EO* the XLF of Pleiades and Hyades had been examined with the improved sensitivity of *ROSAT* (see e.g. Hodgkin et al. 1995; Micela et al. 1996; Pye et al. 1994; Stern et al. 1995). However, all studies of X-ray luminosity on these young clusters were based on smaller data sets than the one presented here.

In lack of the knowledge about individual masses we take account of the known mass dependence of the X-ray luminosity by regarding G, K, and M stars separately. For all spectral type groups wTTS are found to be the strongest X-ray emitters, and the Hyades show the lowest level of X-ray emission. The difference between $\langle L_\mathrm{x}\rangle$ of the Pleiades and the Hyades is small for G stars where the spread in the mass distribution is largest, but large for M stars which have more uniform masses. This suggests that the decline in the X-ray emission is mostly an age effect. The XLF of cTTS and the Pleiades intersect each other, because the Pleiades are characterized by a much steeper distribution indicating less spread in $L_\mathrm{x}$. This difference may be a result of the uniform distance assumed for all stars in a given group (except the Hyades for which individual *Hipparcos* parallaxes were used). If the extension in the direction along the line-of-sight is comparable to the observed spatial dispersion, the TTS in Taurus-Auriga should be subject to a distance spread of ∼50 pc. Consequently the luminosities of some stars are underestimated while others are overestimated, thus leading to a larger spread in $L_\mathrm{x}$ and a flattening of the XLF. For the more compact Pleiades region instead the assumption of uniform distance may be adequate.

The XLF of Hyades K stars show a substructure appearing as an edge at $\log L_\mathrm{x} \sim 28.7$. In order to explain this feature we have divided the K star Hyades into two subgroups of $\log L_\mathrm{x}$ larger/smaller than 28.7. No differences between these two samples were found concerning the distribution of effective temperature, distances, and location on the sky. Only few of the Hyades K stars have measured $v \sin i$ or rotation period. Therefore, the hypothesis that the high-luminosity tail is composed of the fast rotators can not be tested. Note, that the edge in the slope is seen in both single and binary stars (see Fig. 8), but seems to be more pronounced for single stars. We suggest, that the effect is due to as yet undiscovered multiples among the K type Hyades.

We have extended our investigation of the dependence of the X-ray emission on spectral type by direct examination of correlations between these parameters (see Fig. 7). This investigation reveals differences between TTS, Pleiades, and Hyades which we suppose are related to the different ages of these groups. For stars on the MS $T_\mathrm{eff}$ corresponds to mass, and mass is related to the depth of the convection zone. The observed anti-correlation between $\log(L_\mathrm{x}/L_\mathrm{bol})$ and $\log T_\mathrm{eff}$ from Fig. 7 therefore demonstrates the importance of convection for X-ray activity. Although there is a tendency of $\log(L_\mathrm{x}/L_\mathrm{bol})$ being larger for cooler stars, the absolute amount of X-rays emitted is smaller (see Figs. 6 and 7). In the Pleiades $L_\mathrm{x}$ does not strongly depend on spectral type, although $\log(L_\mathrm{x}/L_\mathrm{bol})$ decreases with increasing $T_\mathrm{eff}$. This is most likely due to the shorter time the latest type stars in the Pleiades have spent on the MS. Most of the late K and M type Pleiads did not spin down to loose their high initial activity level, yet. The PMS TTS show no correlation between $\log(L_\mathrm{x}/L_\mathrm{bol})$ and $\log T_\mathrm{eff}$. This may be due to the large age spread in the TTS sample ($10^{5..7}$ yrs).

The most active stars of all groups are characterized by $\log(L_\mathrm{x}/L_\mathrm{bol}) \sim -3$, the canonical value for late-type stars. This behavior is been referred to as "saturation", and has been described in the literature; see e.g. Fleming et al. (1989), Feigelson et al. (1993), Micela et al. (1996), Randich et al. (1996), Stauffer et al. (1997), Micela et al. (1999). A common explanation is that all saturated stars have reached their highest possible level of X-ray activity, e.g. by coverage of the full surface with active regions. The stellar radius rather than rotation would then determine the X-ray emission level (see Fleming et al. 1989). The correlation between $L_\mathrm{x}$ and spectral type in TTS may be understood in terms of such a saturation effect: Fig. 7 suggests that many TTS regardless of their spectral type have reached the saturation level. However, the more luminous the stars, the larger they are, and the higher the saturation level for $L_\mathrm{x}$. Therefore, for given $L_\mathrm{bol}$ the X-ray luminosity is limited by a value that corresponds to saturation, and which is lower for later spectral types.

The dispersion of $\log L_\mathrm{x}$ for given spectral type can be regarded from two points of view: (a) all stars of given spectral type show intrinsically similar amounts of X-ray emission, and the spread in $L_\mathrm{x}$ is caused by variability of individual stars, or (b) the dispersion reflects different activity levels of the stars. Our analysis of the longterm X-ray behavior of these stars (to be presented in a subsequent paper; Stelzer et al. in prep.) suggests little variability on long timescales making the former hypothesis improbable. The distribution of $L_\mathrm{x}$ within stars of homogeneous spectral type thus more likely reflects the variety of X-ray emission from individual stars.

### 6.3. Are Hyades binaries overluminous?

Pye et al. (1994) have examined the XLF of Hyades stars combining 11 *ROSAT* PSPC observations. In their sample they found that Hyades dK binaries are overluminous in X-rays: all binary dK stars analysed by Pye et al. (1994) were brighter than any of the single dK stars. This result was confirmed by Stern et al. (1995) on a larger sample of Hyades drawn from the RASS.

In our analysis of the XLF in the Hyades we have treated binary stars in two ways: (A) in the same way as singles, i.e. without taking account of the multiplicity (sample "b1"), and (B) dividing the observed luminosity

by two to account for X-rays from both components (sample "b2"). We find a probability of ∼10–15% for the null-hypothesis that the distributions of singles ("s") and "b2" among the Hyades K stars are drawn from the same parent distribution. For Hyades M stars (not examined by Pye et al. 1994 due to lack of statistics but found to display a similar though less pronounced divergence between single and binary XLF in the study of Stern et al. 1995) we find a similar probability for the rejection of the null-hypothesis that "s" and "b2" are drawn from the same parent distribution. However, the sample of M star binaries in the Hyades is very small (9 stellar systems). For all other pairs of "s" – "b2" distributions, i.e. those of Hyades G stars, Pleiades, and TTS, there is no statistical evidence for differences. The agreement between the XLF of single ("s") and binary ("b2") stars is expected if the components in binaries have no mutual influence on their activity, and if indeed the distribution of the observed X-ray emission equally on all components conforms with the real situation. This seems likely because binaries with very high mass ratio, i.e. largely different $L_{\rm x}$, are more difficult to detect than equal mass ratio binaries.

When compared to the distributions "b1", singles are fainter in all cases (probability for the distributions being similar <10%). This is in agreement with the study of Pye et al. (1994) and Stern et al. (1995) who have examined samples of type "b1".

This results emphasize that it is important to consider the binary character when analysing XLF of double stars. Splitting the X-ray emission onto the components significantly decreases the difference between single and binary XLF. However, some discrepancy for the Hyades K and M stars remains unexplained. A proper treatment of binary stars is also important in correlation studies, as it decreases the spread.

### 6.4. The age-activity-rotation connection

We have shown that the rotation period and various measures for the X-ray activity (i.e. luminosity, surface flux, and $L_{\rm x}/L_{\rm bol}$-ratio) are correlated for all examined age groups. The steepness of the activity-rotation relation is very different for TTS, Pleiades, and Hyades, with the largest slope for the TTS, e.g. slow rotators in the Pleiades have much higher surface flux than TTS with similar periods (see Figs. 9 to 11). We think that these differences can be explained by the particular distribution of spectral types: In Fig. 12 we show the $\log F_{\rm s} - \log P_{\rm rot}$ diagrams with plotting symbols scaled according to $T_{\rm eff}$. In the TTS sample we observe a clear clustering of cooler stars at slow rotation periods. For given $L_{\rm bol}$ and $L_{\rm x}$ cooler stars have larger radius and therefore smaller surface flux. This results in a steeper slope for the TTS sample.

Fast rotators are found at all spectral types in the Pleiades and among the TTS. Indeed, the fastest rotators form the upper envelope to the $\log(L_{\rm x}/L_{\rm bol})$–$\log T_{\rm eff}$ diagram (Fig. 7). At the age of the Hyades most stars (regardless of spectral type) have slowed down their rotation, such that the range of measured periods is limited, and definitive statements about the activity-rotation connection for the Hyades are difficult.

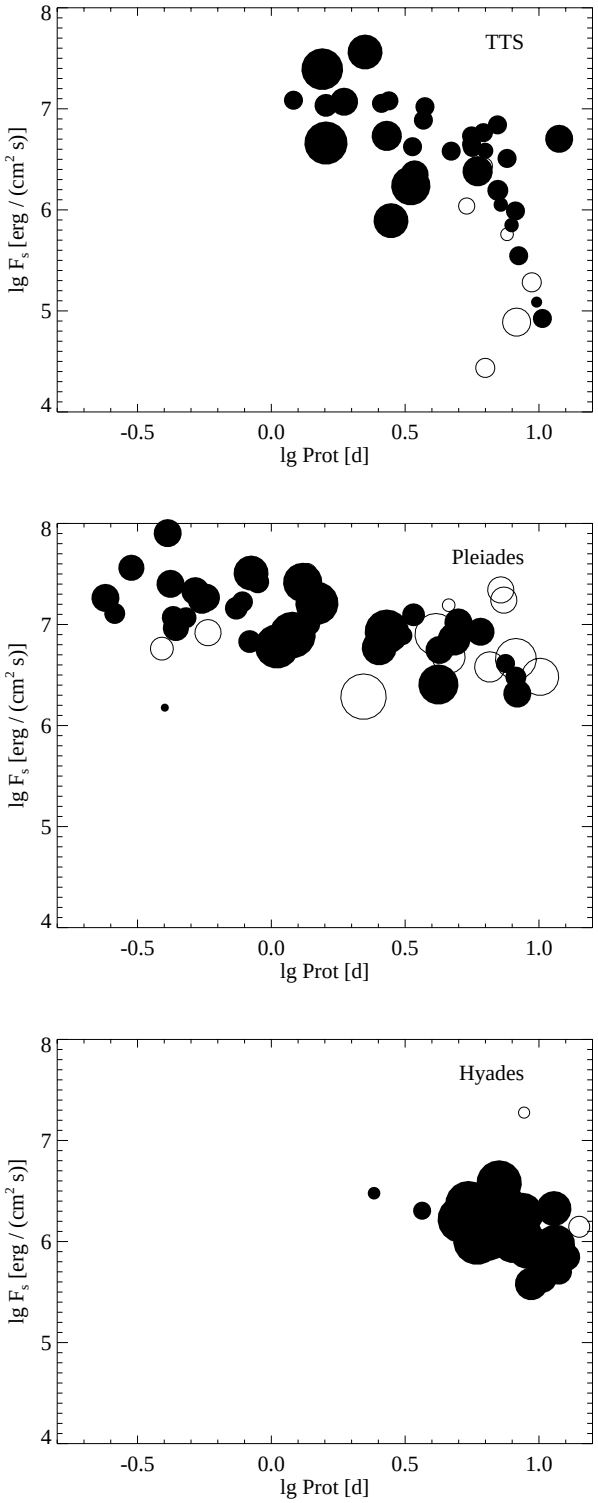


**Fig. 12.** X-ray surface flux versus rotation period for TTS, Pleiades, and Hyades indicating the distribution of effective temperatures (plotting symbols are scaled to $T_{\rm eff}$). Note, that most of the slow rotators in the TTS sample are cool objects. Open circles are upper limits for undetected objects.

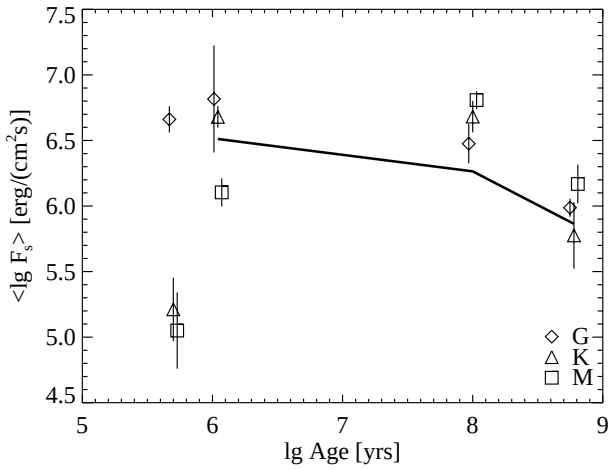


**Fig. 13.** Time evolution of the X-ray surface flux for TTS, Pleiades, and Hyades for three spectral type groups (plotting symbols for G and M stars for clarity with a small offset on the age-scale). The thick solid line represents a fit to the mean of $F_s$ obtained by combining G, K, and M stars from the wTTS, Pleiades, and Hyades sample. The slope of this exponential decay is $-2.0 \pm 0.1$ in agreement with earlier estimates for smaller samples of stars from the same region (see text).

We have examined the mean level of X-ray surface flux for each age group in order to infer a decay law. In Fig. 13 the mean $F_s$ is plotted for cTTS, wTTS, Pleiades, and Hyades, each being split into G, K, and M type stars. The X-ray flux increases from cTTS to wTTS as mentioned by N95. (Only one cTTS has spectral type of G.) An exponential fit to the combined G + K + M sample from the wTTS to the Hyades age is overlaid, and provides a slope of $-2.01 \pm 0.09$. This compares well with the result by Walter & Barry (1991) who found a decrease of $F_s$ with $-2.20 \pm 0.21$ for a sample composed of *Einstein* detected naked TTS, Pleiades and Hyades.

*Acknowledgements.* We made use of the Open Cluster Database, compiled by C. F. Prosser and J. R. Stauffer. R.N. wishes to acknowledge financial support from the Bundesministerium für Bildung und Forschung through the Deutsche Zentrum für Luft- und Raumfahrt e.V. (DLR) under grant number 50 OR 0003. The *ROSAT* project is supported by the Max-Planck-Gesellschaft and Germany's federal government (BMBF/DLR). We would like to thank the referee T. Montmerle for helpful comments and stimulating discussions.

## References

Alcalá, J. M., Krautter, J., Covino, E., et al. 1997, A&A, 319, 184
Baraffe, I., Chabrier, G., Allard, F., & Hauschildt, P. H. 1998, A&A, 337, 403
Bouvier, J. 1990, AJ, 99, 946
Bouvier, J., Cabrit, S., Fernández, M., Martín, E. L., & Matthews, J. M. 1993, A&A, 272, 176
Bouvier, J., Forestini, M., & Allain, S. 1997a, A&A, 326, 1023
Bouvier, J., Wichmann, R., Grankin, K., et al. 1997b, A&A, 318, 495
Casanova, S., Montmerle, T., Feigelson, E. D., & André, P. 1995, ApJ, 439, 752
Cernicharo, J., Bachiller, R., & Duvert, G. 1985, A&A, 149, 273
Cruddace, R. G., Hasinger, G. R., & Schmitt, J. H. M. M. 1988, in Astronomy from large databases, ed. F. Murtagh, A. Heck (ESO, Garching), 177
Damiani, F., Micela, G., & Vaiana, G. S. 1991, in Angular Momentum Evolution of Young Stars, NATO Adv. Research Workshop held in Noto, Sicily, Italy, ed. S. Catalano, & J. R. Stauffer (Kluwer, Dordrecht), 89
Damiani, F., & Micela, G. 1995, ApJ, 446, 341
Damiani, F., Micela, G., Sciortino, S., & Harnden, Jr. F. R. 1995, ApJ, 446, 331
D'Antona, F., & Mazzitelli, I. 1994, ApJS, 90, 467
Edwards, S., Strom, S. E., Hartigan, P., et al. 1993, AJ, 106, 372
Elias, J. H. 1978, ApJ, 224, 857
Feigelson, E. D., & Nelson, P. I. 1985, ApJ, 293, 192
Feigelson, E. D., & Kriss, G. A. 1989, ApJ, 338, 262
Feigelson, E. D., Casanova, S., Montmerle, T., et al. 1993, ApJ, 416, 623
Fleming, T. A., Gioia, I. M., & Maccacaro, T. 1989, ApJ, 340, 1011
Fleming, T. A., Molendi, S., Maccacaro, T., et al. 1995, ApJS, 99, 701
Gagné, M., & Caillault, J.-P. 1995, ApJ, 445, 280
Grankin, K. N. 1993, IBVS, 3823
Grosso, N., Montmerle, T., Bontemps, S., et al. 2000, A&A, 359, 113
Hearty, T. J., Neuhäuser, R., Stelzer, B., et al. 2000, A&A, 353, 1044
Herbig, G. H., & Bell, K. R. 1988, Lick Observatory Bulletin, No. 1111
Hodgkin, S. T., Jameson, R. F., & Steele, I. A. 1995, MNRAS, 274, 869
Isobe, T., Feigelson, E. D., & Nelson, P. I. 1986, ApJ, 306, 490
Kenyon, S. J., & Hartmann, L. 1995, ApJS, 101, 117
König, B., Neuhäuser, R., & Stelzer, B. 2001, A&A, 369, 971
Koenigl, A. 1991, ApJ, 370, L39
LaValley, M., Isobe, T., & Feigelson, E. 1992, in Astronomical Data Analysis Software and Systems I, ed. D. M. Worrall et al., ASP Conf. Ser. 25, 245
Leggett, S. K., & Hawkins, M. R. S. 1989, MNRAS, 238, 145
Luhman, K. L. 2000, ApJ, 544, 1044
Martín, E. L. 1997, A&A, 321, 492
Martín, E. L., Montmerle, T., Gregorio-Hetem, J., & Casanova, S. 1998, MNRAS, 300, 733
Mermilliod, J. C., Turon, C., Robichon, N., et al. 1997, in ESA Symposium Hipparcos Venice 98, Venice, Italy, ed. B. Battrick, ESA SP-402, 643
Micela, G., Sciortino, S., Kashyap, V., et al. 1996, ApJS, 102, 75
Micela, G., Sciortino, S., Harnden, Jr. F. R., et al. 1999, A&A, 341, 751
Montmerle, T., Koch-Miramond, L., Falgarone, E., & Grindlay, J. E. 1983, ApJ, 269, 182
Neuhäuser, R., Sterzik, M. F., Schmitt, J. H. M. M., et al. 1995, A&A, 297, 391 (N95)
Neuhäuser, R., & Comerón, F. 1998, Science, 282, 83
Neuhäuser, R., Briceño, C., Comerón, F., et al. 1999, A&A, 343, 883
Palla, F., & Stahler, S. W. 1999, ApJ, 525, 772

Pallavicini, R., Golub, L., Rosner, R., et al. 1981, ApJ, 248, 279
Paresce, F. 1984, AJ, 89, 1022
Perryman, M. A. C., Brown, A. G. A., Lebreton, Y., et al. 1998, A&A, 331, 81
Preibisch, T. 1997, A&A, 324, 690
Preibisch, T., Zinnecker, H., & Herbig, G. H. 1996, A&A, 310, 456
Pye, J. P., Hodgkin, S. T., Stern, R. A., et al. 1994, MNRAS, 266, 798
Randich, S., Schmitt, J. H. M. M., Prosser, C. F., & Stauffer, J. R. 1996, A&A, 305, 785
Reid, I. N., & Hawley, S. L. 1999, AJ, 117, 343
Ryter, C. E. 1996, Ap&SS, 236, 285
Schmidt-Kaler, T. H. 1982, Physical Parameters of Stars, in Landolt-Börnstein New Ser., Vol 2b, Astronomy and Astrophysics Stars and Star Clusters, ed. K. Shaifers, & H. H. Voigt (New York, Springer)
Schmitt, J. H. M. M. 1985, ApJ, 293, 178
Skumanich, A. 1972, ApJ, 171, 565
Stassun, K. G., Mathieu, R. D., Mazeh, T., & Vrba, F. J. 1999, AJ, 117, 2941
Stauffer, J. R., Caillault, J.-P., Gagné, M., Prosser, C. F., & Hartmann, L. W. 1994, ApJS, 91, 625
Stauffer, J. R., Hartmann, L. W., Prosser, C. F., et al. 1997, ApJ, 479, 776
Stelzer, B., Neuhäuser, R., & Hambaryan, V. 2000, A&A, 356, 949 (SNH00)
Strom, K. M., & Strom, S. E. 1994, ApJ, 424, 237
Stern, R. A., Schmitt, J. H. M. M., Pye, J. P., et al. 1994, ApJ, 427, 808
Stern, R. A., Schmitt, J. H. M. M., & Kahabka, P. T. 1995, ApJ, 448, 683
Walter, F. M. 1981, ApJ, 245, 677
Walter, F. M., & Bowyer, S. 1981, ApJ, 245, 671
Walter, F. M. 1982, ApJ, 253, 745
Walter, F. M. 1983, ApJ, 274, 794
Walter, F. M., Brown, A., Mathieu, R. D., Myers, P. C., & Vrba, F. J. 1988, AJ, 96, 297
Walter, F. M., & Barry, D. C. 1991, in The sun in time, ed. C. P. Sonnett et al. (Tucson, Univ. Arizona Press), 663
Wichmann, R., Krautter, J., Schmitt, J. H. M. M., Neuhäuser, R., Alcalá, J. M., et al. 1996, A&A, 312, 439
Wichmann, R., Bastian, U., Krautter, J., et al. 1998a, MNRAS, 301, L39
Wichmann, R., Bouvier, J., Allain, S., & Krautter, J. 1998b, A&A, 330, 521